https://ntrs.nasa.gov/search.jsp?R=19930087638 2020-06-17T09:19:33+00:00Z

NACA RM L53E27

NACA

RESEARCH MEMORANDUM

TEST OF AN AERODYNAMICALLY HEATED MULTIWEB WING STRUCTURE (MW-1) IN A FREE JET AT MACH NUMBER 2

By Richard R. Heldenfels, Richard Rosecrans,
and George E. Griffith

Langley Aeronautical Laboratory
Langley Field, Va.

NATIONAL ADVISORY COMMITTEE
FOR AERONAUTICS

WASHINGTON

July 30, 1953

NATIONAL ADVISORY COMMITTEE FOR AERONAUTICS

RESEARCH MEMORANDUM

TEST OF AN AERODYNAMICALLY HEATED MULTIWEB WING STRUCTURE (MW-1) IN A FREE JET AT MACH NUMBER 2

By Richard R. Heldenfels, Richard Rosecrans, and George E. Griffith

SUMMARY

A multiweb wing structure, representing an airplane or missile wing, was tested under simulated supersonic flight conditions to determine the transient temperature distribution. The aerodynamic loads played an important and unanticipated role, however, in that the model experienced a dynamic failure near the end of the test. The test is discussed and the conclusion reached that the model failed as a result of the combined action of aerodynamic heating and loading. The temperature data collected are analyzed and are shown to be in reasonable agreement with calculated values.

INTRODUCTION

As part of an investigation of the structural effects of aerodynamic heating, the Structures Research Division of the Langley Laboratory is testing complex structures, representative of airplane or missile wings, under aerodynamic conditions similar to supersonic flight. The first such test had as its purpose the experimental determination of the transient temperature distribution throughout a small multiweb wing structure. Only temperatures were measured on the model during this exploratory test; however, the aerodynamic loads played an important and unanticipated role in that the model experienced a dynamic failure near the end of the test. The test program is now proceeding to additional models on which temperatures, strains, and static pressures are being measured.

Because of the interest exhibited in the failure of the model, this paper has been prepared to describe the test and indicate the probable causes of failure. The temperature-distribution data collected are also presented and compared with calculated results.

SYMBOLS

c	specific heat, Btu/(lb)(°F)
h	heat-transfer coefficient, Btu/(sq ft)(sec)(°F)
H	stagnation pressure, psia
k	thermal conductivity, Btu/(ft)(sec)(°F)
t	time from start of air flow, sec
t_o	time of initial conditions in temperature calculations, sec
T	model temperature, °F
T_o	initial model temperature, °F
T_{AW}	adiabatic wall temperature, °F
T_S	stagnation temperature, °F
w	specific weight, lb/cu ft
τ	skin thickness, ft

APPARATUS

Preflight Jet

The test was conducted in the preflight jet of the Langley Pilotless Aircraft Research Station at Wallops Island, Va. This facility is a blow-down type wind tunnel that incorporates a heat accumulator for stagnation temperature control. (See ref. 1.) Various nozzles can be attached to provide a range of Mach numbers and free-jet areas in which to test models. A nominal Mach number two, 27- by 27-inch nozzle was used for this particular test. Stabilized aerodynamic conditions can be maintained at the exit of this nozzle for about 9 seconds after a 2-second starting period.

Model

The model designated MW-1 was a somewhat idealized section of a multi-web wing having no taper in plan form or thickness ratio (see fig. 1) and

a 5-percent-thick, symmetrical circular-arc airfoil section. The model was of 40-inch chord and span and had 0.125-inch-thick skin, six 0.072-inch-thick internal webs and solid leading- and trailing-edge pieces $4\frac{1}{8}$ inches wide, all made of 24S-T3 aluminum alloy. The webs were spaced $5\frac{1}{4}$ inches apart and solid steel bulkheads were located at each end of the model, the root bulkhead being welded to a mounting fixture. Doubler plates were added near the mounting fixture to strengthen the root connection. The model was designed for ease of construction and testing; thus, the configuration used is not necessarily an efficient multiweb structure.

Instrumentation

Model temperatures were measured by 22 iron-constantan thermocouples installed in the skin, webs, and leading- and trailing-edge members at the locations shown in figure 2. Thermocouples were peened into small holes drilled in the metal and the remaining cavities were filled with Sauereisen cement. The leads extended down inside the model and were carried out through holes in the root bulkhead.

Test conditions were determined from measurements of the stagnation pressure and stagnation temperature of the jet. Stagnation pressure was measured by total-pressure tubes located in the settling chamber and connected to pressure transducers. Stagnation temperature was measured by chromel-alumel thermocouples mounted on a rake downstream of the heat accumulator.

All data were recorded on three 18-channel oscillographs synchronized so that matching timing marks were recorded on all films. Films were read in an oscillogram projector and the deflections so measured were converted to temperatures or pressures by using the individual calibration curves of the recording channels. Model instrumentation was supplemented by a 16-millimeter motion-picture camera running at 24 frames per second. This camera was not equipped with any special timing device or synchronized with the recorders.

Accuracy

The over-all reliability of the data is affected by several sources of error that include the installation and characteristics of the sensing elements, measuring circuits, recording elements, and reading device. In addition, all measurements were of a transient nature so that the combined response rate of the pickups and recorder must be considered. The estimated maximum errors in individual measurements are as listed below along with the time constants for a step function input. These values were

obtained by adding the errors of the various contributing factors but, since it is unlikely that errors from all sources were a maximum simultaneously, the probable error should be substantially less than the following:

	Accuracy	Time constant
Stagnation pressures	±2.6 psi	0.03 sec
Stagnation temperature	±16° F	1.0 sec
Model temperatures	±14° F	.03 sec

The Mach number, as determined by calibration tests, was 1.99 ± 0.01.

Errors due to the thermocouple installation have not been included above, but they are believed to be small since the thermocouples were completely surrounded by metal. In addition, the thermocouples may not have measured the average skin temperature since there was a small temperature difference (less than 6° F) through the thickness. Consequently, the skin thermocouples, located at the midplane of the skin, should record the average skin temperature within 1° to 2°.

Description of Test

The model was mounted vertically in the jet at a nominal angle of attack of 0° and with its leading edge 1 inch downstream of the nozzle exit plane. (See figs. 2 and 3.) The model extended completely through the jet with the tip extending 4 inches above and the root 9 inches below the airstream. Thus, about two-thirds of the span was within the jet with the bulkheads and root connection being outside the jet. The top of the model was stabilized by guy cables attached near both the leading and trailing edges.

The average aerodynamic conditions obtained during the test were: Mach number, 1.99; stagnation temperature, 556° F; and stagnation pressure, 115 psia. These conditions are discussed in greater detail in the next section.

As the jet control valve was opened, the stagnation pressure built up quickly, reached the desired level in less than 2 seconds, and then fluctuated about that level for the remainder of the test. The model survived the starting shock without sign of trouble and apparently remained stationary until about 7.5 seconds after the jet started. At this time a vibratory motion began and the model was soon destroyed. The first evidence

of trouble was buckling of the skin panels near the leading edge. These buckles appeared and disappeared rapidly, moving toward the trailing edge. At 8.1 seconds, the cable guys at the top had shaken loose and a buckle had settled in the most rearward skin panel which then failed at about 8.8 seconds. The trailing-edge piece blew away at about 9.0 seconds and was followed by successive disintegration until complete destruction at about 9.9 seconds.

The process described is illustrated in figure 4 by six frames selected from the motion picture, and the remains of the model after the test are shown in figure 5. The times given in figure 4 and in the above description were obtained by correlating the movie with the recorders by means of the times at which the various thermocouples failed and should be considered approximate.

RESULTS AND DISCUSSION

Aerodynamic Data

The variation of stagnation pressure with time is given in figure 6. Since the stagnation pressure fluctuated during the run, test conditions were never stabilized; however, an average value of the test stagnation pressure was determined by integrating the curve of H against t between $t = 1.5$ and $t = 8.0$ seconds.

In figure 7, the stagnation-temperature curves show a time variation, but this variation is attributed to the relatively slow response of the stagnation thermocouples. A more unsatisfactory feature is the spread indicated by the stagnation thermocouples. The accuracy with which these thermocouples report the average stagnation temperature of the jet is unknown since no surveys have been made at the nozzle exit. For lack of better data, the arithmetic average of the individual stagnation thermocouples was used as the test stagnation temperature.

The average test conditions are listed below along with other pertinent aerodynamic data:

Angle of attack (nominal), deg	0
Mach number	1.99
Stagnation pressure, psia	115
Static pressure, psia	15.0
Dynamic pressure, psi	41.5
Stagnation temperature, $^{\circ}F$	556
Free-stream temperature, $^{\circ}F$	107
Speed of sound, ft/sec	1.17×10^3
Free-stream velocity, ft/sec	2.32×10^3
Free-stream density, slugs/cu ft	2.22×10^{-3}
Reynolds number	42.5×10^6

Model Temperatures

The temperatures measured at 22 locations on the model are plotted against time in figure 8 which also contains calculated results to be discussed later. Data are presented for only eight seconds of the run since all thermocouples began to give erratic readings shortly thereafter. In these and all other plots, time is reckoned from the instant that air began to flow through the jet. All curves show a flat portion at the beginning of the test while the jet is starting; after the full test conditions are attained, the temperatures rise more or less rapidly, depending on their location. At the end of the test, all temperatures were climbing at a substantial rate so that the temperature distribution was still transient and far from the steady state.

The skin temperatures were the highest model temperatures recorded, as would be expected. At any given time, the skin temperature decreases from the leading edge to the trailing edge since the rate at which heat is transferred from the boundary layer to the model decreases with distance from the leading edge. A decrease along the span from top to bottom is also in evidence and may be due to an uneven distribution of temperature in the jet, although heat conduction into the heavy base may have some effect on thermocouple 13.

The interior temperatures are always less than that of the adjacent skin and at the end of the test were increasing at their highest rate, whereas the rate of increase of the skin temperature had begun to drop. The interior temperatures also exhibit a longer lag between the start of the test and the beginning of the temperature rise. Furthermore, the distance from the surface affects the temperature so that the lowest interior temperature at any given time is found at the center of the web just back of the thickest point (thermocouple 16). The above effects are to be expected and reflect the time required to conduct heat over varying distances from the surface to the interior, as well as the variation of heat transfer with distance from the leading edge.

Temperature — Time-History Calculations

Two types of temperature calculations are considered in this section: (1) simple calculations of skin temperatures at those locations that are practically unaffected by heat conduction to the internal structure and (2) detailed calculations of the temperature distribution for a complete chordwise cross section of the model. The results of the skin-temperature calculations did not agree well with the test results, and, when investigated, this discrepancy was found to be due to theoretical values of the adiabatic wall temperature being somewhat higher than the values indicated by the test results. Adjusted values of T_{AW} were then used in the more detailed calculations and generally good agreement was obtained between

the measured and calculated temperatures at both the skin and interior thermocouple locations. A discussion of these calculations follows.

Skin temperatures (calculation A).- Skin temperatures were calculated assuming that temperature variation through the skin thickness, heat flow by conduction to other parts of the model, and radiant heat transfer could be neglected. The point heat balance between the heat absorbed by an element of the skin and the heat transferred from the boundary layer results in the following differential equation:

$$\frac{dT}{dt} + \frac{h}{c w \tau} T = \frac{h}{c w \tau} T_{AW} \tag{1}$$

The heat-transfer coefficient h and adiabatic wall temperature T_{AW} were calculated from the turbulent-flow formulas given in reference 2 using parameters determined from local flow conditions just outside the boundary layer. Local flow conditions were calculated by a shock-expansion analysis of two-dimensional supersonic flow around a circular-arc airfoil in a uniform jet. The variation of stagnation pressure during the test had a negligible effect on the heat transfer except during the starting phase so that the starting phase was neglected and the average test conditions were used for the remainder of the test. The values thus obtained for h and T_{AW} vary across the chord of the model and are shown as the theoretical curve in figure 9.

The specific heat c of 24S-T3 aluminum alloy was assumed to be constant during the test. The structural parameters appearing in equation (1) are as follows: c, 0.23 Btu/(lb)($^{\circ}$F); w, 173 lb/cu ft; τ, 0.0104 ft.

In this analysis, the terms $\frac{h}{c w \tau}$ and T_{AW} are constants so that the solution of equation (1) is

$$T = T_{AW} - \left(T_{AW} - T_o\right) e^{-\frac{h(t-t_o)}{c w \tau}} \tag{2}$$

where T_o is the temperature of the skin element at the time t_o. In evaluating equation (2), T_o was taken as 50° F, the average temperature of the model just before the test, while t_o was taken as 0.7 second to allow for the variation of test conditions during the starting phase.

The results given by equation (2) for skin thermocouples located sufficiently far from any internal structure to be unaffected by heat

flow along the skin, numbers 2, 4, 6, 10, 11, 12, 13, 15, 17, 19, and 21, have been plotted in figure 8 and are marked calculation A. These results are seen to be consistently higher than the experimental results. The source of disagreement must be in the heat-transfer coefficients or adiabatic wall temperature or both; therefore an investigation was made to determine the source of this discrepancy.

"Indicated" values of h and T_{AW}.- If the test had run long enough, the skin temperatures would have stabilized and conclusive values of T_{AW} could have been obtained. But, since this was not the case, some other approach had to be used. When $h/c_{w\tau}$ and T_{AW} are constants, equation (1) is a linear equation in the variables T and dT/dt. "Indicated" values of h and T_{AW} can then be obtained from a plot of T against dT/dt, a straight line that intercepts the T axis at T_{AW} and has a slope the magnitude of which is the quantity $c_{w\tau}/h$.

Constant test conditions were nearly obtained, so the above method should be applicable to the experimental temperature histories. The data from all skin thermocouples, except 7 and 14 which may be influenced by heat conduction into the nearby web, were so analyzed by using the method of least squares to fit a straight line to the experimental points. Figure 10 is a sample plot of T against dT/dt and shows that the method is indeed applicable since the test points follow a straight line. The results of this analysis are plotted in figure 9, along with the theoretical values, as a function of distance from the leading edge. The group of points 20 inches from the leading edge give values obtained from the thermocouples (10, 11, 12, 13, and 15) distributed along the span of the model, but individual points have not been identified since there were no significant trends.

The "indicated" heat-transfer coefficients agree well with the theoretical values on the leading half of the chord; whereas the agreement for the adiabatic wall temperatures is not so good. For both, the results are rather erratic in the trailing half, a result that can be attributed to the size of the model. The model was so large that the trailing half was in a region of nonuniform flow and thus the data in this region are somewhat questionable. This uncertainty is also reflected by plots of T against dT/dt for thermocouples 17, 19, and 21 in that they exhibited much more scatter than is shown in figure 10.

The poor agreement between theoretical and "indicated" adiabatic wall temperatures on the leading half of the chord, and thus recovery factors, may be partly due to the uncertainty involved in the determination of the average test stagnation temperature (see fig. 7). The "indicated" recovery factors obtained on the leading half of the model (0.68 to 0.76) are even lower than that expected in laminar flow, and laminar flow should not prevail on the model except near the leading edge because of the high

local Reynolds numbers and the inherent turbulence of the jet. If the theoretical turbulent flow recovery factor (0.894) and the "indicated" adiabatic wall temperature are used to determine the stagnation temperature, values between 450° and 490° F. are obtained; these values are below the minimum measured stagnation temperature. Therefore, some unknown factor in the test apparently resulted in a low recovery factor. Radiant heat transfer from the model is one source of low recovery factors but this effect was investigated and found negligible.

It is pertinent to note, in addition, that calculated skin temperature histories for such a short test can be made to agree well with the experimental data by any one of several combinations of adjustments to h and T_{AW}. The curves for T against t, in the time range of interest, are apparently rather insensitive to changes in h and T_{AW}; however, if such curves are examined on a plot of T against dT/dt, the differences may be clearly seen. The above leads to the conclusion that calculation A did not agree well with the test data because the theoretical adiabatic wall temperature was higher than that indicated by the test data.

Temperature distributions (calculation B).- A temperature history for a complete chordwise cross section of the model was obtained from a calculation that took into consideration the conduction of heat along the skin and down into the internal structure. The model cross section was divided into eight segments with the dividing line between segments being chosen so that heat conduction along the skin at these points could be considered negligible. Temperature distributions were then calculated for each of the segments by using a numerical process similar to that of reference 3. For this numerical calculation, the segments for the solid leading and trailing edges with the attached skin were each subdivided into 16 elements whereas the other segments for skin and web combinations were each subdivided into 12 elements. The theoretical values of h were used in these calculations; however, T_{AW} was taken equal to 446° F (an average value indicated by the test data) to improve the agreement between test and calculations. The thermal conductivity of the 24S-T3 aluminum alloy was taken as a constant 0.0188 Btu/ft/sec/°F.

In figure 8, the temperature histories thus calculated are compared to individual experimental histories for thermocouples located in the skin, webs, and leading- and trailing-edge members. Fairly good agreement between calculated and experimental values can be seen for both the skin and interior temperatures. The better agreement between the measured skin temperatures and calculation B than with calculation A can be attributed to the use of an adjusted T_{AW} rather than to the inclusion of heat-conduction effects. The interior temperatures are consistently overestimated; this overestimation may be due to thermal resistance of the riveted joints or may possibly be due to the use of approximate values

of the thermal properties of the material, particularly the thermal conductivity. The value of specific heat used appears sufficiently accurate as evidenced by the good agreement between indicated and theoretical heat-transfer coefficients.

For the leading-edge segment, as shown in figure 11, temperatures are given for both 4 and 8 seconds for the center line of the solid section and for the skin. The two experimental points show fairly good agreement with the calculations, although interior temperatures are overestimated, possibly because of some thermal resistance offered by the joint between the skin and the solid section. Although calculated center-line temperatures for the solid section were plotted to compare directly with the experimental values, the calculated surface temperatures directly above this point never exceeded the center-line temperature by more than 15° F.

Similar temperature distributions for the skin and web combination, third from the leading edge, are given in figure 12 for both 4 and 8 seconds. The combined thickness of skin and web flange, where they are in contact, was used in the computations. Fairly good agreement exists between the calculated and experimental temperatures, but, as discussed previously in regard to figure 8, calculation B overestimates the true web temperatures.

Figure 13 shows the chordwise distributions at 4 and 8 seconds for the skin temperatures and the temperatures at the center line of the solid leading and trailing edges and of the webs. The test data are seen to be in fairly good agreement with the calculations. Figure 13 illustrates the effect of the internal structure on the skin temperature distribution and that, even at the lower temperatures shown at 4 seconds, appreciable differences exist between the surface and interior temperatures.

Model Failure

The model was designed to withstand static aerodynamic loads imposed by angles of attack up to 2.5° and, although no special consideration had been given to its dynamic characteristics or the induced thermal stresses, the model was expected to survive the test. The limited information obtained about the failure has since been analyzed, but the exact cause of failure has not been established; additional tests, however, are in progress to investigate further the observed phenomena. Certain conclusions have been reached about the nature and probable causes of failure, however, and they will now be discussed.

The primary cause of failure must have been the rapid heating or the model would have shown some sign of distress earlier in the test. The immediate cause of failure was apparently skin buckling.

One effect of rapid heating on the model is a reduction of material properties such as strength and stiffness. The short time the model was exposed to elevated temperatures, however, could cause only small reductions in these material properties; thus, this effect must have been of secondary importance with regard to the failure.

Another, and more important, effect of the rapid heating is that substantial thermal stresses are induced in the model by the nonuniformity of this heating. These thermal stresses are the only significant stresses present that could cause skin buckling. An adequate thermal stress analysis of the model would involve more temperature data than are available and require very tedious and lengthy computations; therefore, only approximate analyses, using the methods of reference 4, have been made. These analyses showed that, in the spanwise direction, the maximum direct stress in the skin was near the leading edge and had a magnitude of about 30 percent of the critical spanwise compressive stress. These spanwise direct stresses are the result of the temperature differences between the internal structure and the skin. In the chordwise direction, compressive stresses are induced because that portion of the model outside the jet, including the heavy steel bulkheads, restrains the thermal expansion of the hot skin of the model. Calculations show that these stresses could be of the same order of magnitude as the critical chordwise compressive stress (ref. 5). Orders of magnitude only are mentioned because of the approximations involved in calculating the stress distribution and in determining the restraints which influence the critical stresses. Further evidence that chordwise compression caused the buckling is that the buckles were long and narrow, the type produced by transverse compression of long plates. If spanwise compression had been the cause, a series of small circular buckles would have appeared in each skin panel. The above considerations thus show that chordwise compressive stresses, due to restrained thermal expansion, were the probable cause of skin buckling but they do not provide any indications of why the failure occurred in the vicinity of the trailing edge. (A study of the thermal buckling of flat plates is reported in ref. 6.)

The failure was a dynamic phenomenon in that the buckling was not steady. The buckling started near the leading edge (the region of maximum heating) and then seemed to appear and disappear in several locations before settling in the most rearward panel. This latter buckle may not have been stationary despite the fact that the film so indicated, since the buckling frequency could have been such that the camera showed a stationary condition. Other vibrations were also in evidence for the guy cables at the top of the model were shaken loose, but no data are available to indicate the mode or frequency of such vibrations.

The dynamic aspect of the failure indicates that the model experienced some form of flutter. The visible evidence shows that the principal effect was more of a localized flutter than an over-all torsion or bending-type flutter. Such considerations point to panel flutter as a possibility. Some recent experimental data on panel flutter (ref. 7) show that a buckled panel is more apt to flutter than an unbuckled one, a condition that ties in with the test results. The data of reference 7 are not directly applicable to the present test, but it is of interest to investigate the panel flutter parameter of the model. If the distance between webs is used as the panel length, then the panel flutter parameter falls far off scale in the stable region of the plots in reference 7. A panel length in excess of half the model chord would be required to get a panel flutter parameter of small enough magnitude to fall in the transition region of figure 7 of reference 7. Thus, the case for panel flutter is not on very firm ground although some form of flutter was most likely a factor in the failure.

The indications are that the failure was the result of the combined effects of aerodynamic heating and loading. The rapid aerodynamic heating induced thermal buckling of the model skin which in turn led to an unstable aeroelastic condition. The final result was a dynamic failure that may have been a form of localized flutter. The test clearly demonstrates that there is much to be learned about the individual and combined effects of aerodynamic heating and loading on aircraft structures and that, when these effects are not simultaneously considered, factors which vitally affect the structural integrity of an aircraft may be overlooked.

CONCLUSIONS

A multiweb wing structure has been tested under aerodynamic conditions representing flight at Mach number 2, stagnation temperature of 556° F, and stagnation pressure of 115 psia, with the following results:

1. Model temperatures rose rapidly during the test as a result of aerodynamic heating. The skin near the leading edge experienced the most rapid heating, with the rate decreasing toward the trailing edge. The temperatures of the internal structure lagged behind those of the adjacent skin panels because of the distance through which heat had to be conducted to these parts. The heat sinks formed by the internal structure lowered the skin temperatures in their immediate vicinity.

2. Detailed calculations of the temperature distribution on a complete chordwise cross section of the model are found to be in generally good agreement with the test data if an "indicated" adiabatic wall temperature, somewhat lower than that predicted by theory, is used.

3. The model failed near the end of the test as a result of the combined action of aerodynamic heating and loading. The rapid aerodynamic heating apparently induced thermal buckling of the model skin which in turn led to an unstable aeroelastic condition. The final result was a dynamic failure that appeared to be some form of flutter.

4. Much remains to be learned about the individual and combined effects of aerodynamic heating and loading on aircraft structures and, when these effects are not considered simultaneously, factors which vitally affect the structural integrity of an aircraft may be overlooked.

Langley Aeronautical Laboratory,
National Advisory Committee for Aeronautics,
Langley Field, Va., May 13, 1953.

REFERENCES

1. Faget, Maxime A., Watson, Raymond S., and Bartlett, Walter A., Jr.: Free-Jet Tests of a 6.5-Inch-Diameter Ram-Jet Engine at Mach Numbers of 1.81 and 2.00. NACA RM L50L06, 1951.

2. Chauvin, Leo T., and deMoraes, Carlos A.: Correlation of Supersonic Convective Heat-Transfer Coefficients From Measurements of the Skin Temperature of a Parabolic Body of Revolution (NACA RM-10). NACA RM L51A18, 1951.

3. Kaye, Joseph: The Transient Temperature Distribution in a Wing Flying at Supersonic Speeds. Jour. Aero. Sci., vol. 17, no. 12, Dec. 1950, pp. 787-807, 816.

4. Heldenfels, Richard R.: The Effect of Nonuniform Temperature Distributions on the Stresses and Distortions of Stiffened-Shell Structures. NACA TN 2240, 1950.

5. Batdorf, S. B., Stein, Manuel, and Libove, Charles: Critical Combinations of Longitudinal and Transverse Direct Stress for an Infinitely Long Flat Plate With Edges Elastically Restrained Against Rotation. NACA WRL-49, 1946. (Formerly NACA ARR L6A05a.)

6. Gossard, Myron L., Seide, Paul, and Roberts, William M.: Thermal Buckling of Plates. NACA TN 2771, 1952.

7. Sylvester, Maurice A., and Baker, John E.: Some Experimental Studies of Panel Flutter at Mach Number 1.3. NACA RM L52I16, 1952.

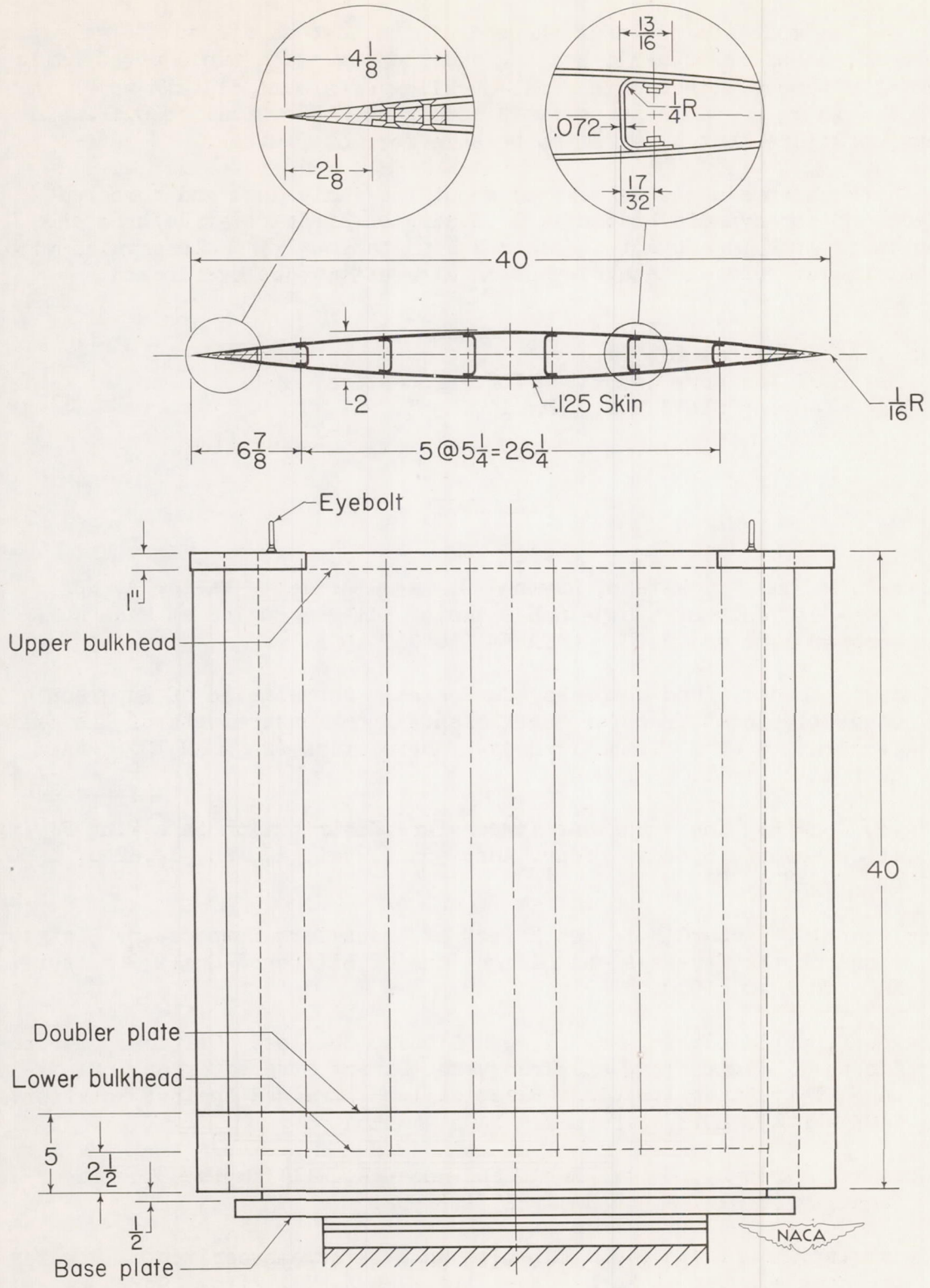

Figure 1.- Dimensions of multiweb wing model MW-1.

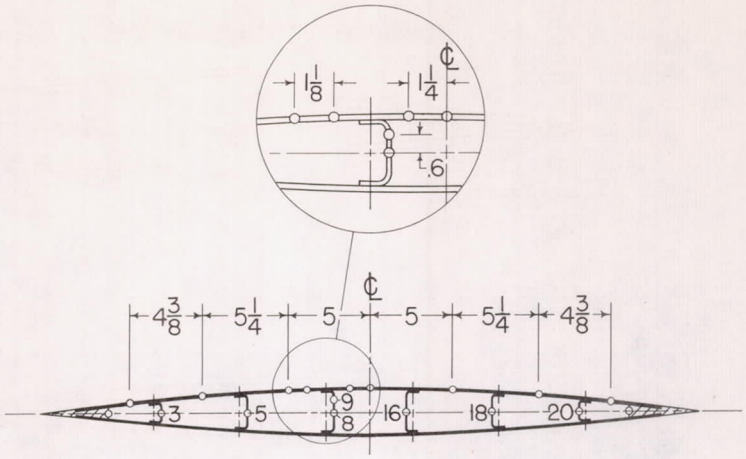

(a) Chordwise section along jet center line.

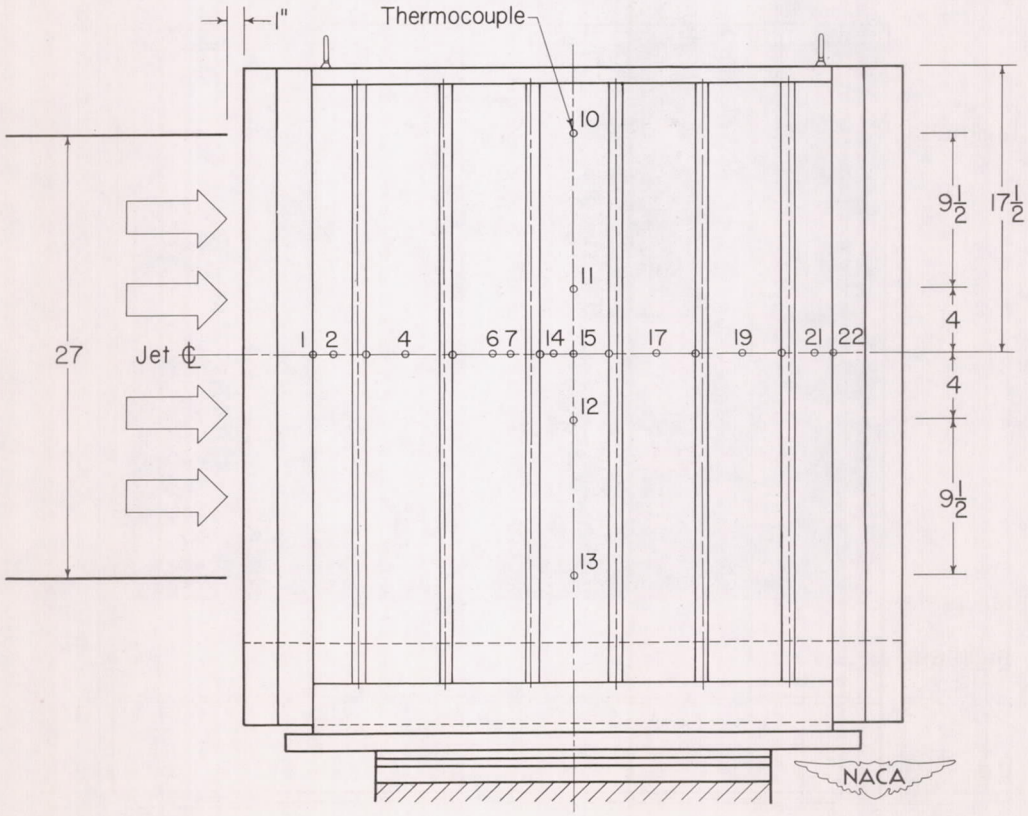

(b) Side view with near skin removed.

Figure 2.- Locations and numbers of thermocouples.

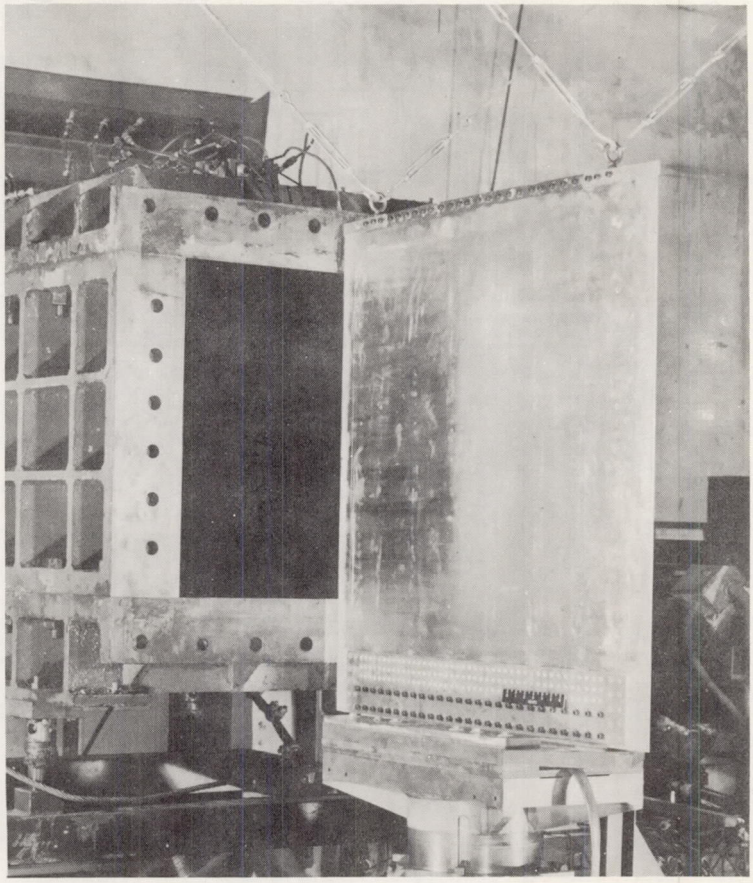

NACA
L-74844

Figure 3.- Model in place at nozzle exit prior to test.

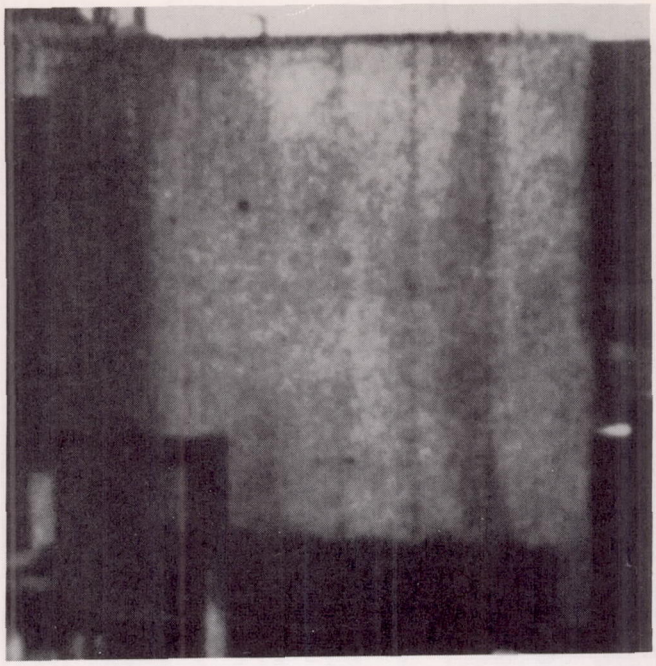

NACA L-79266

(a) t = 8.1 sec.

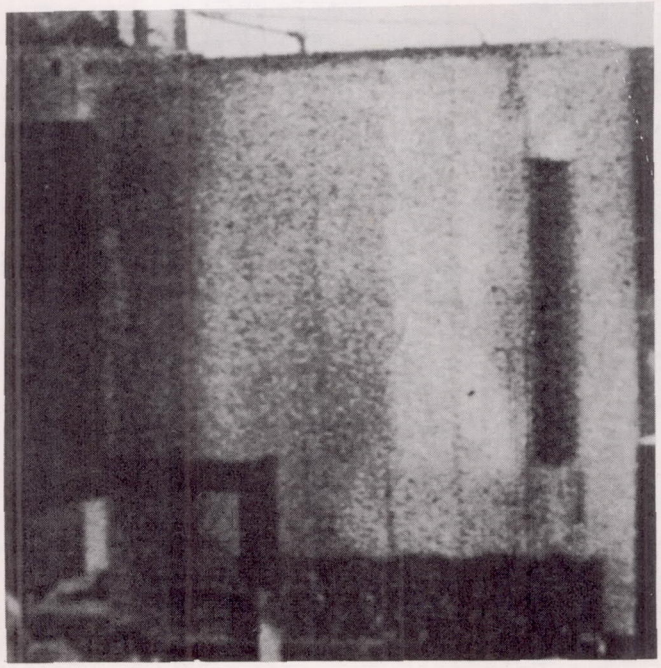

NACA L-79267

(b) t = 8.8 sec.

Figure 4.- Progressive failure of model (taken from motion picture).

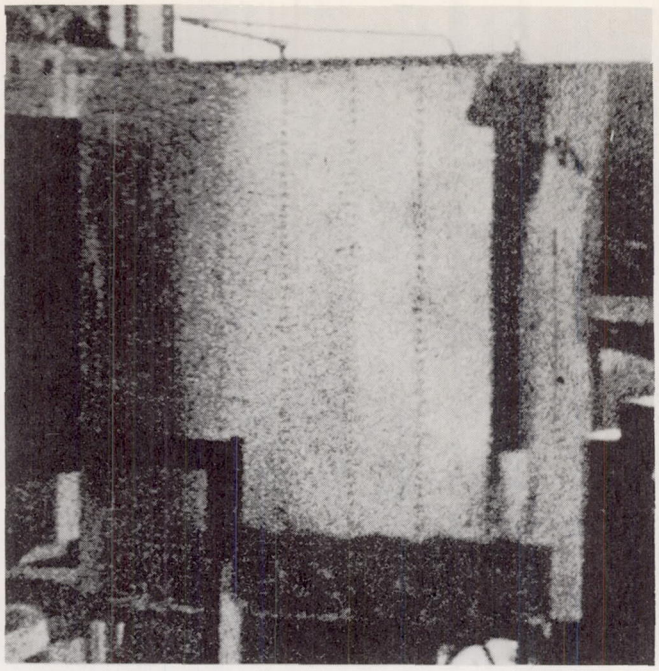

NACA

(c) t = 8.9 sec. L-79268

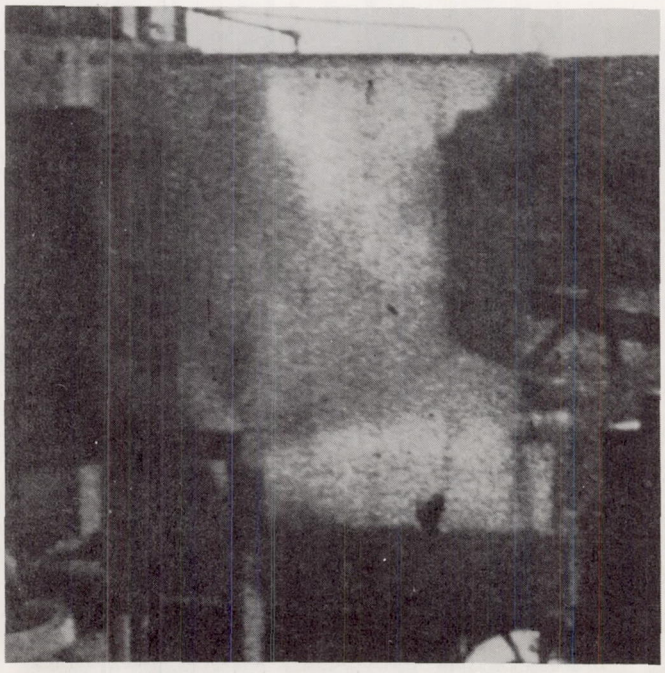

NACA

(d) t = 9.2 sec. L-79269

Figure 4.- Continued.

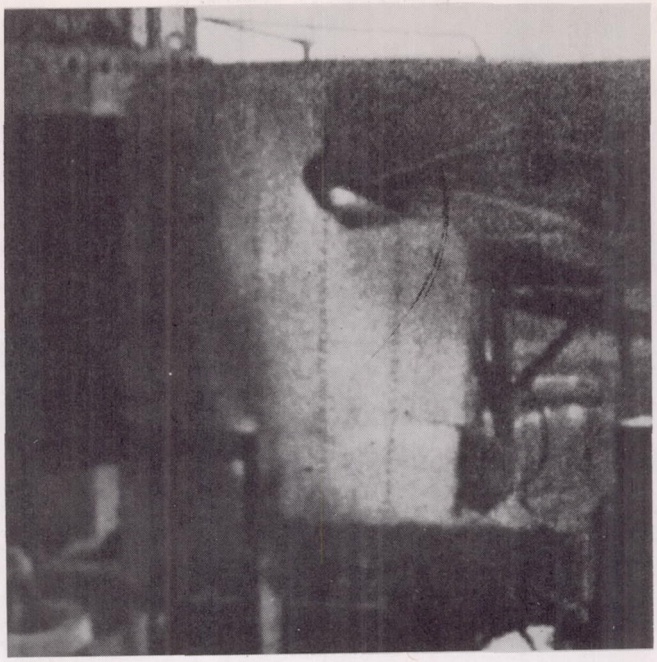

NACA L-79270

(e) t = 9.7 sec.

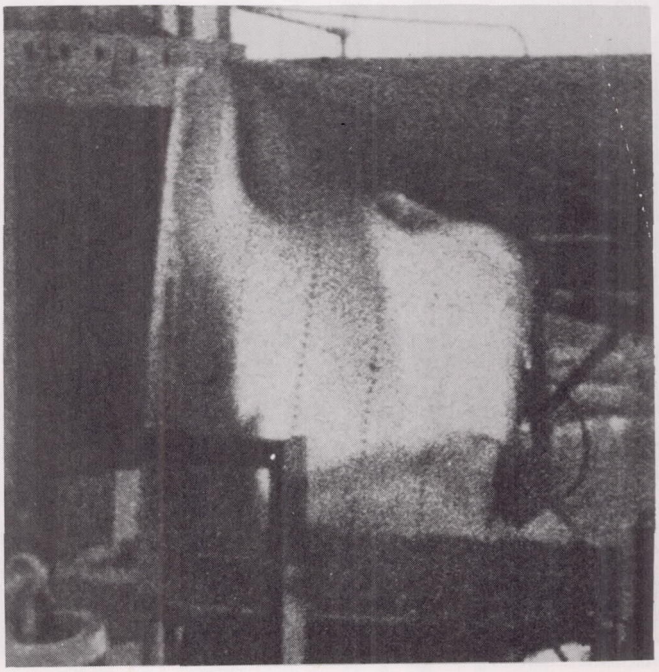

NACA L-79271

(f) t = 9.8 sec.

Figure 4.- Concluded.

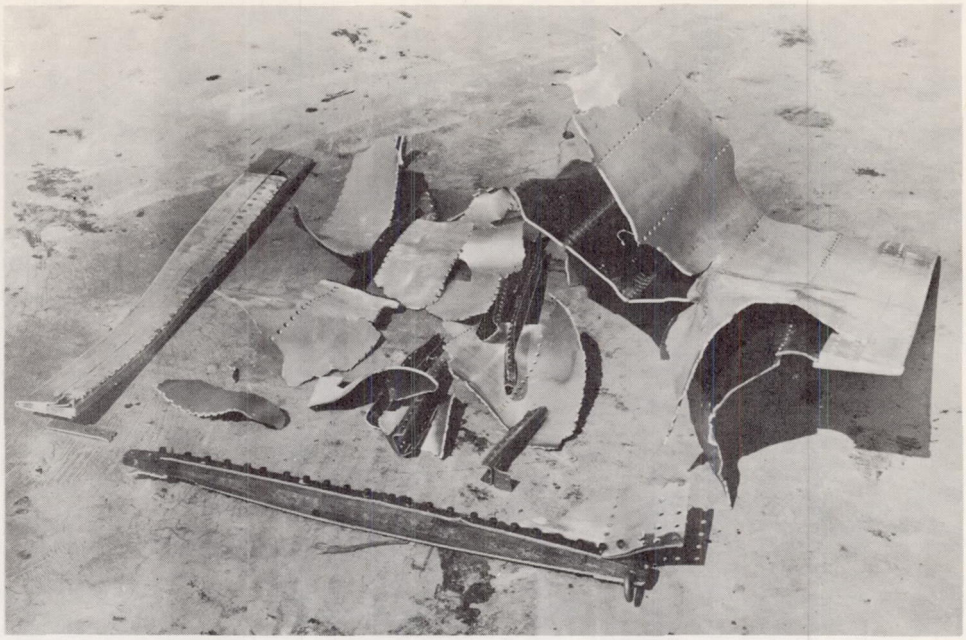

(a) Pieces separated during test.

NACA
L-74847

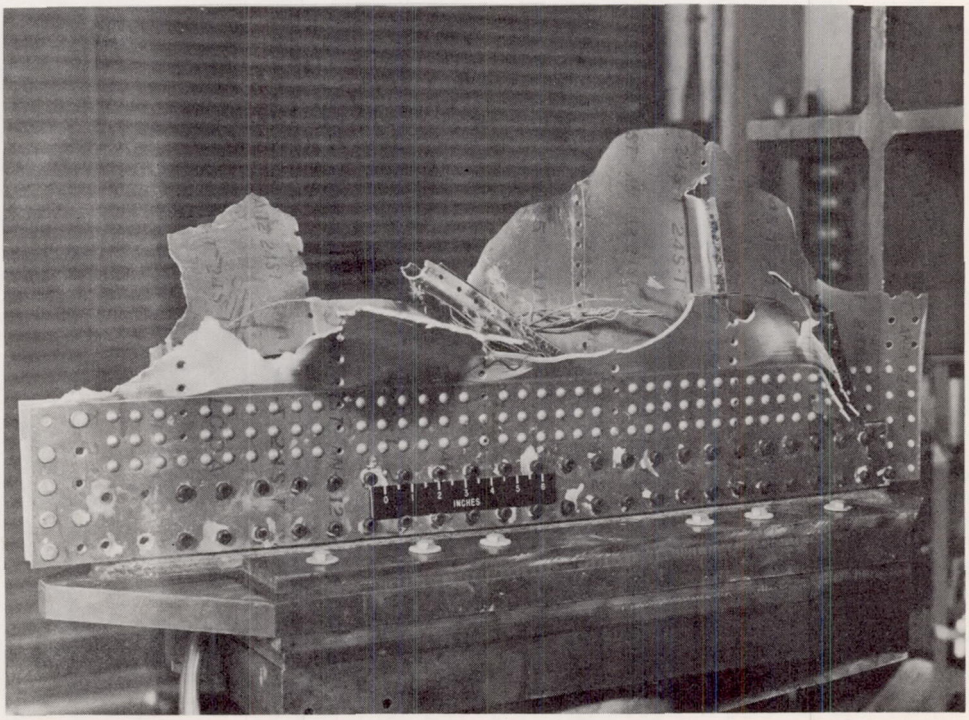

(b) Pieces attached to mounting fixture.

NACA
L-74845

Figure 5.- Remains of model after test.

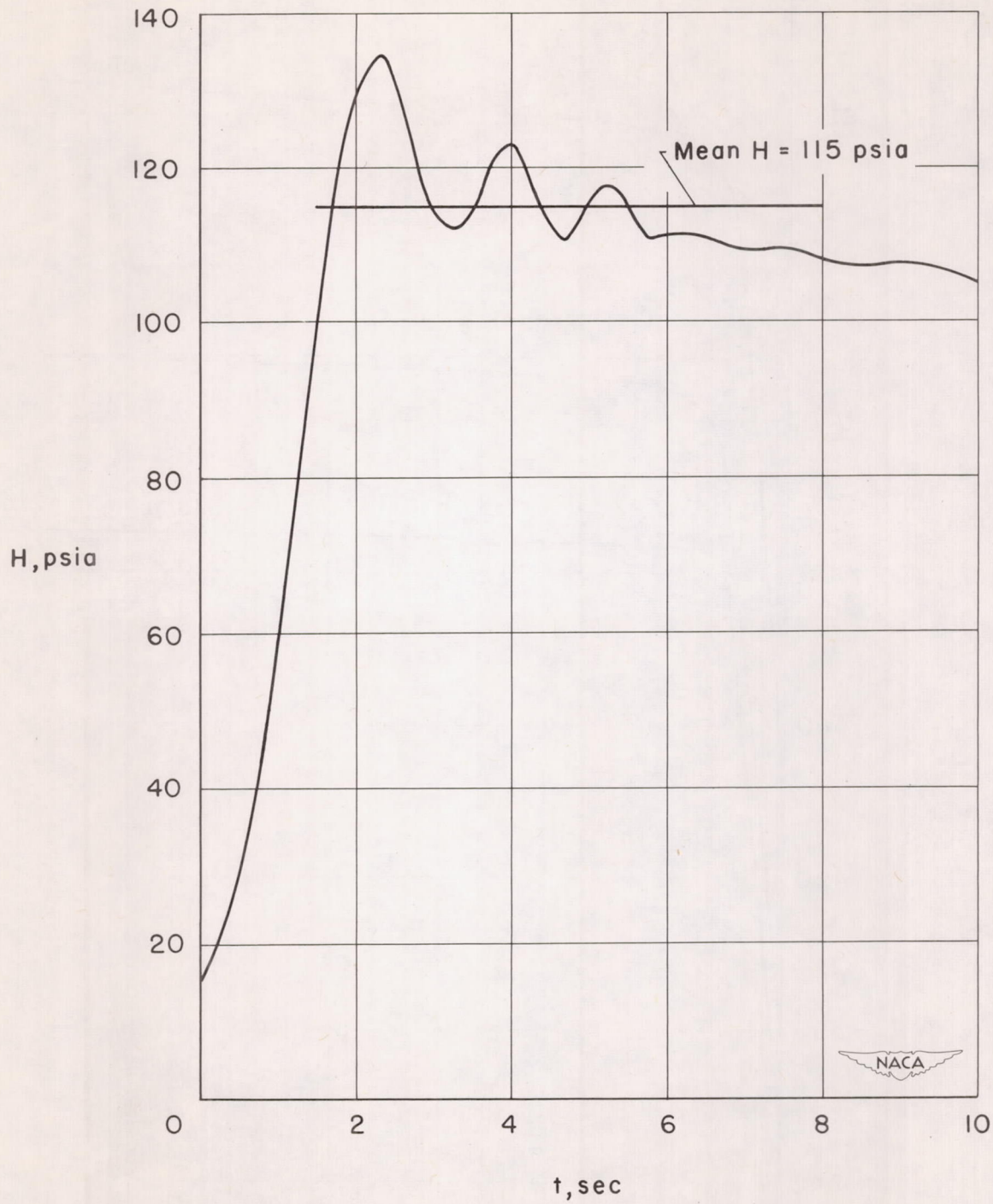

Figure 6.- Variation of stagnation pressure during test.

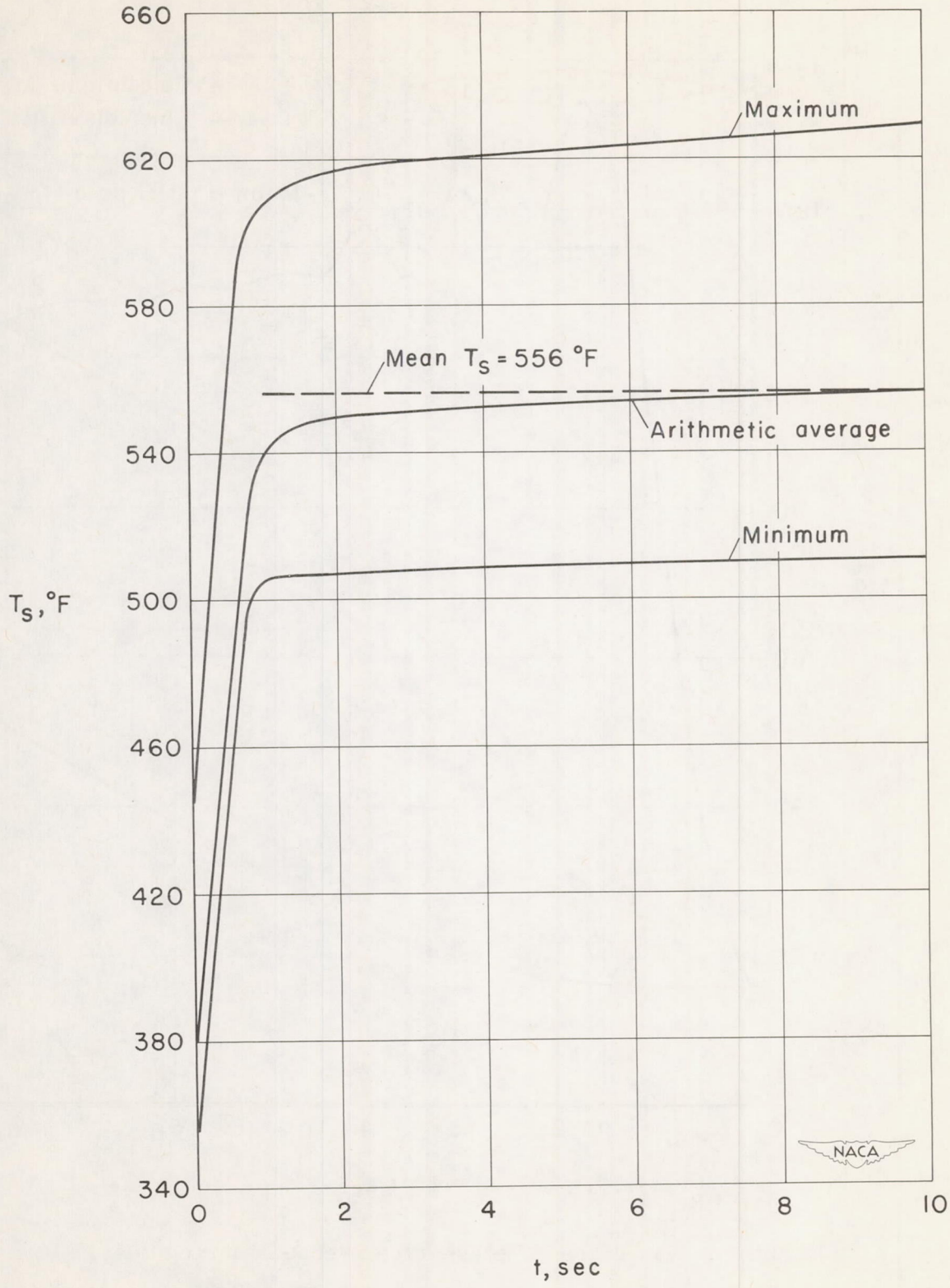

Figure 7.- Variation of stagnation temperature during test.

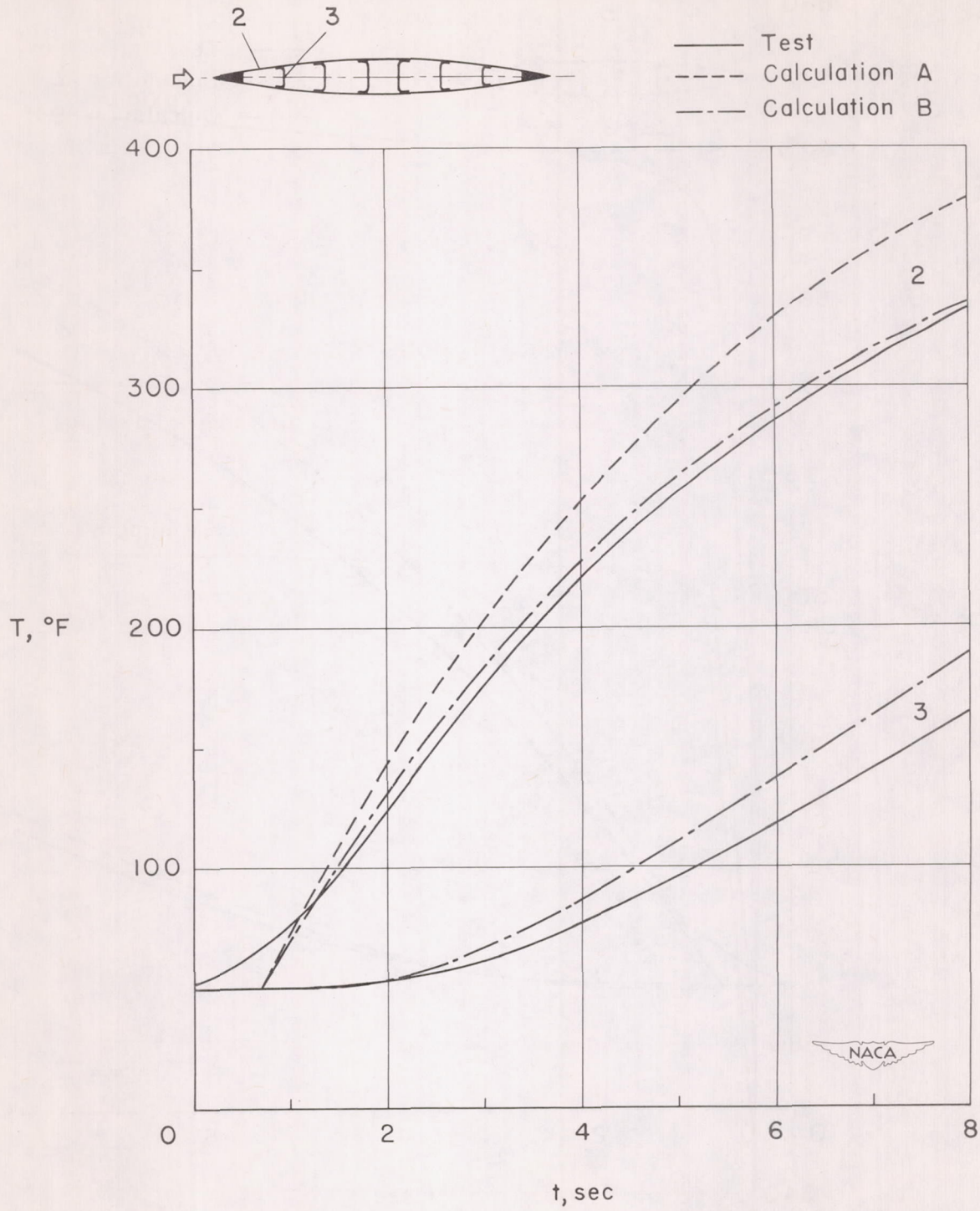

(a) Thermocouples 2 and 3.

Figure 8.- Variation of model temperatures during test.

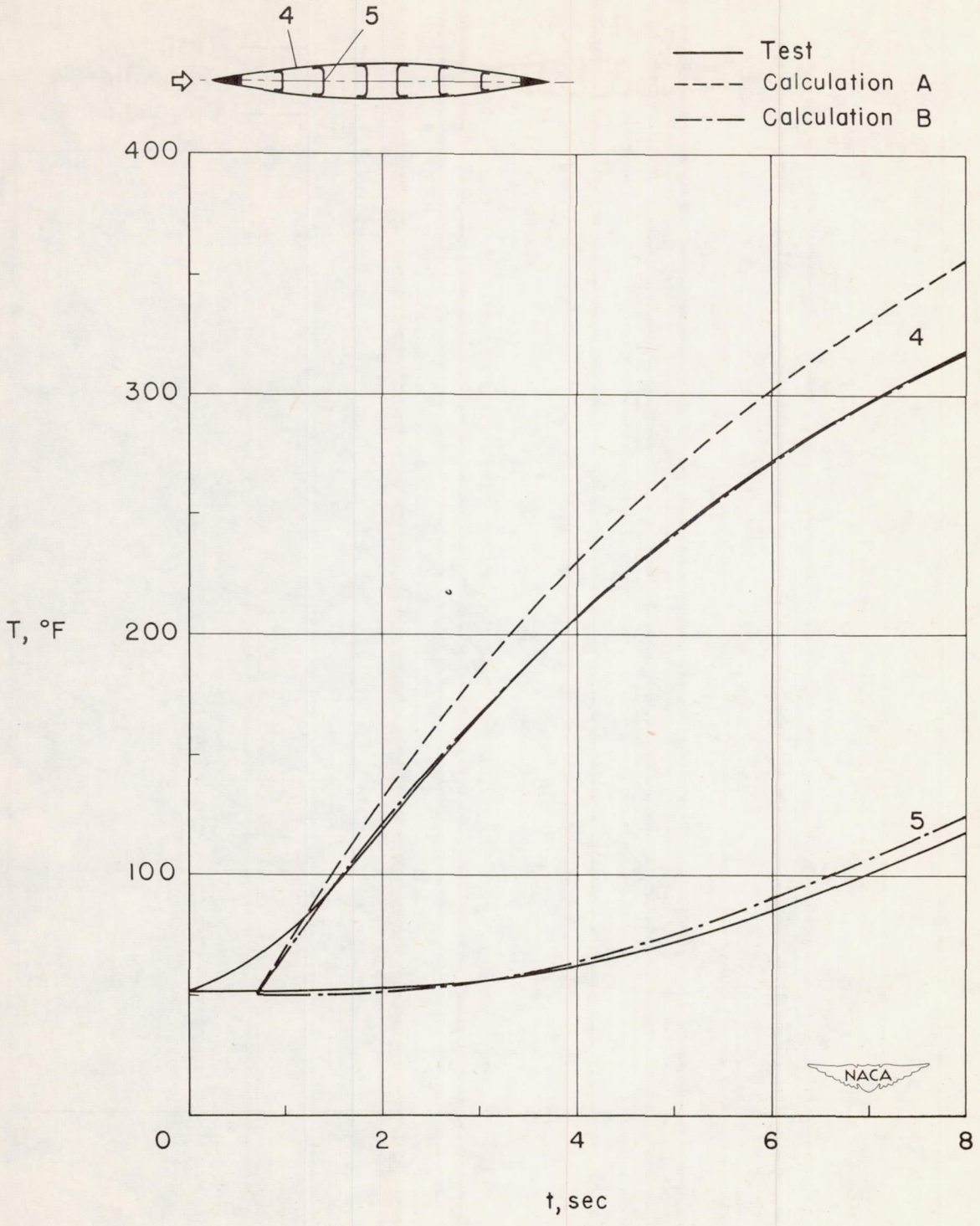

(b) Thermocouples 4 and 5.

Figure 8.- Continued.

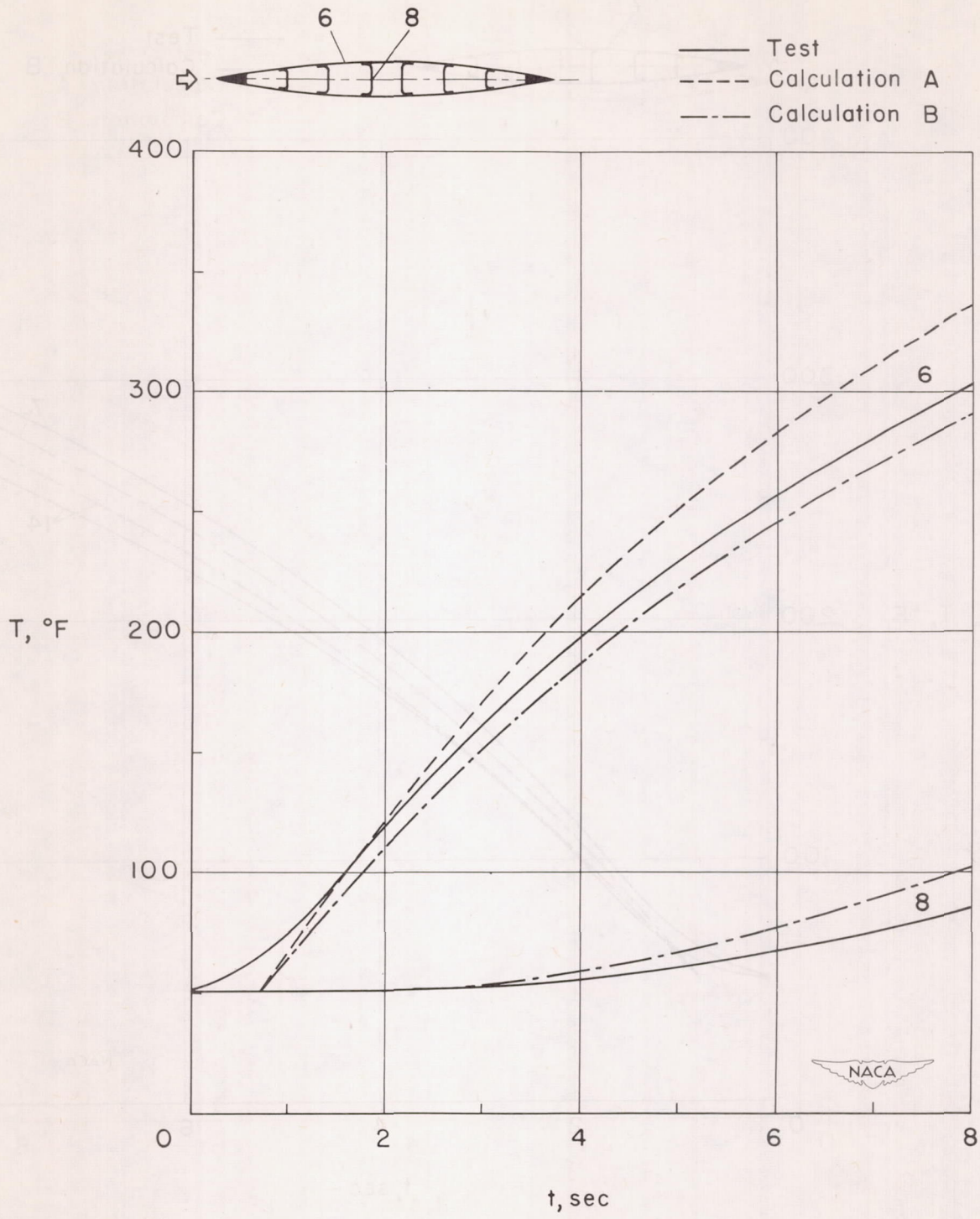

(c) Thermocouples 6 and 8.

Figure 8.- Continued.

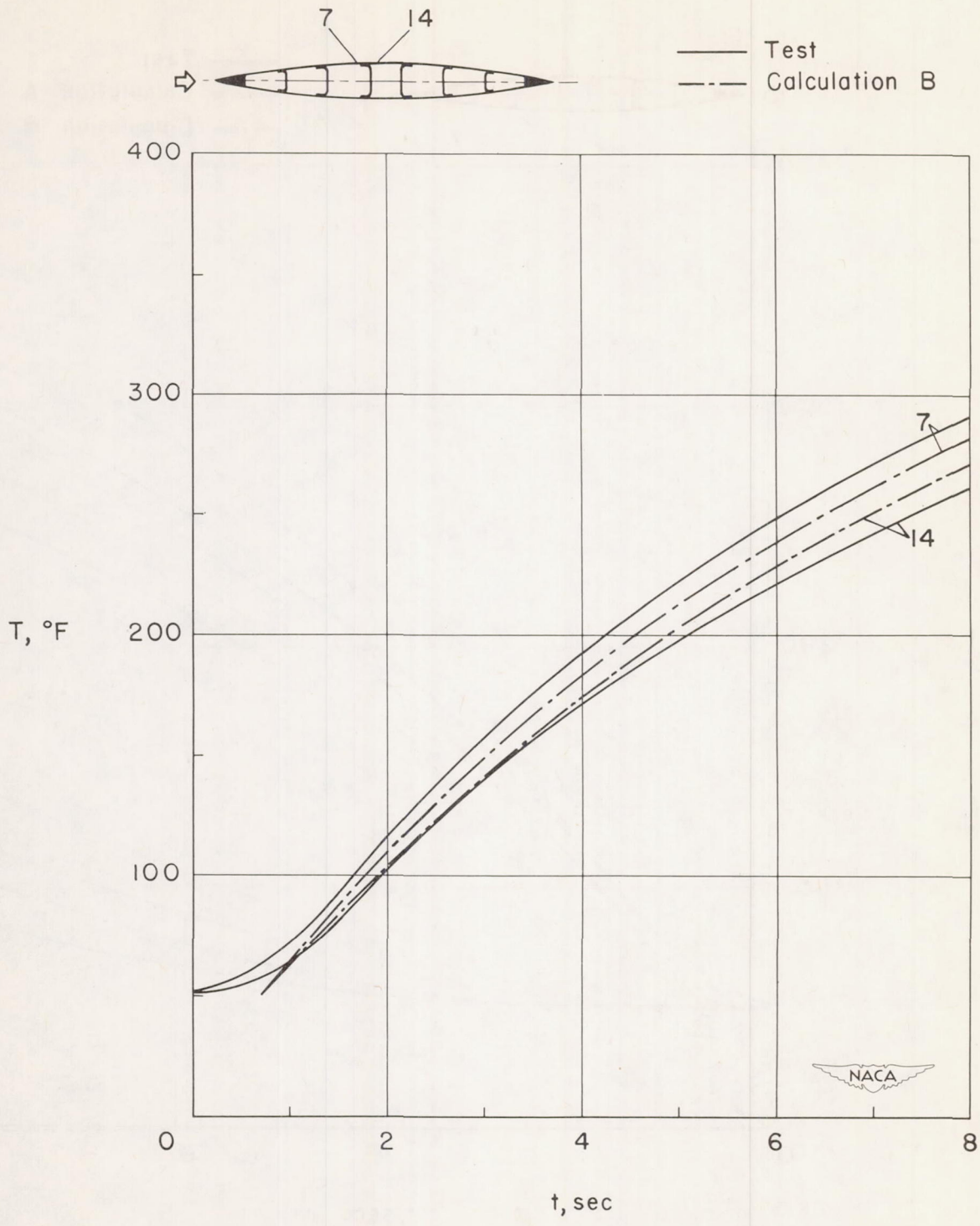

(d) Thermocouples 7 and 14.

Figure 8.- Continued.

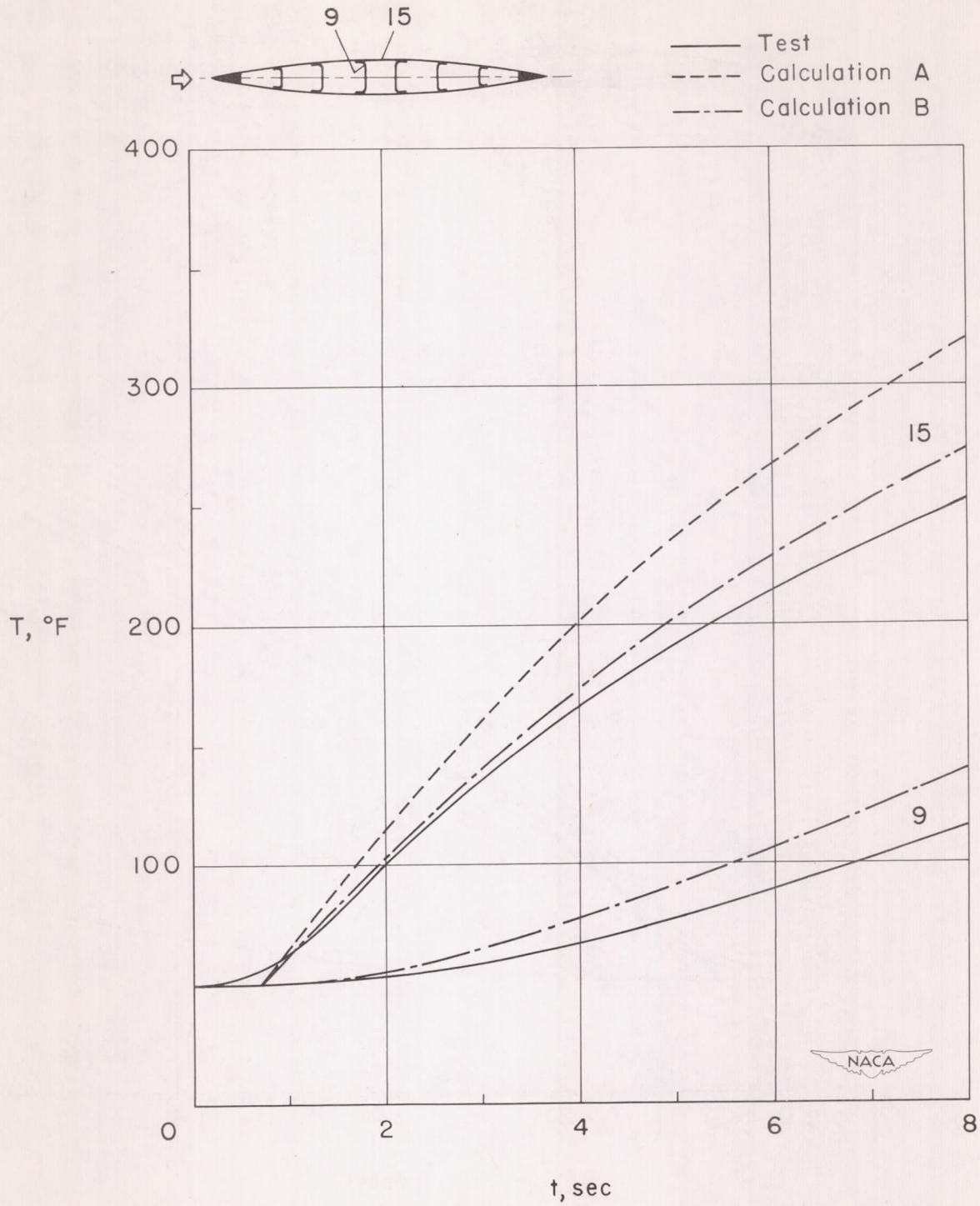

(e) Thermocouples 9 and 15.

Figure 8.- Continued.

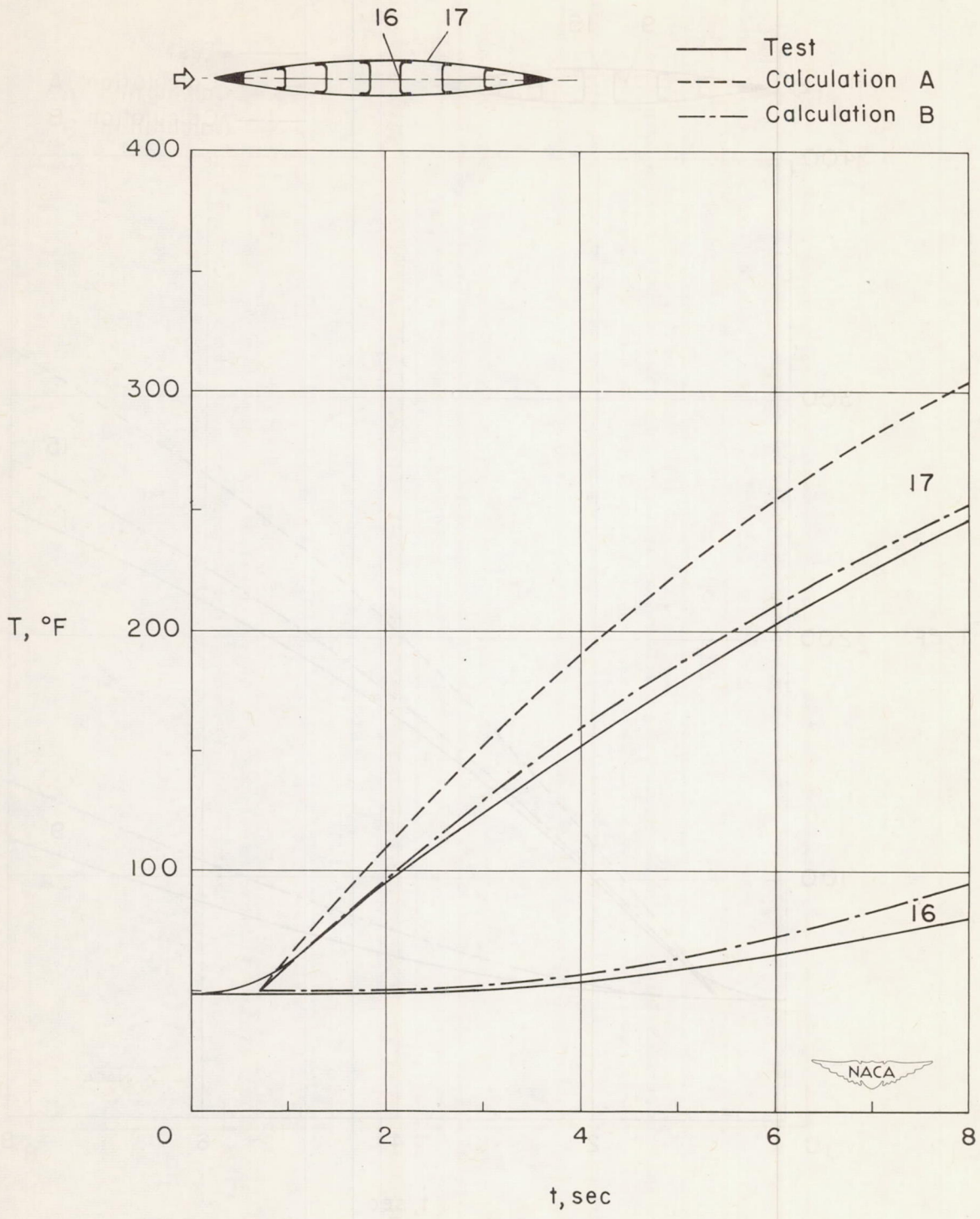

(f) Thermocouples 16 and 17.

Figure 8.- Continued.

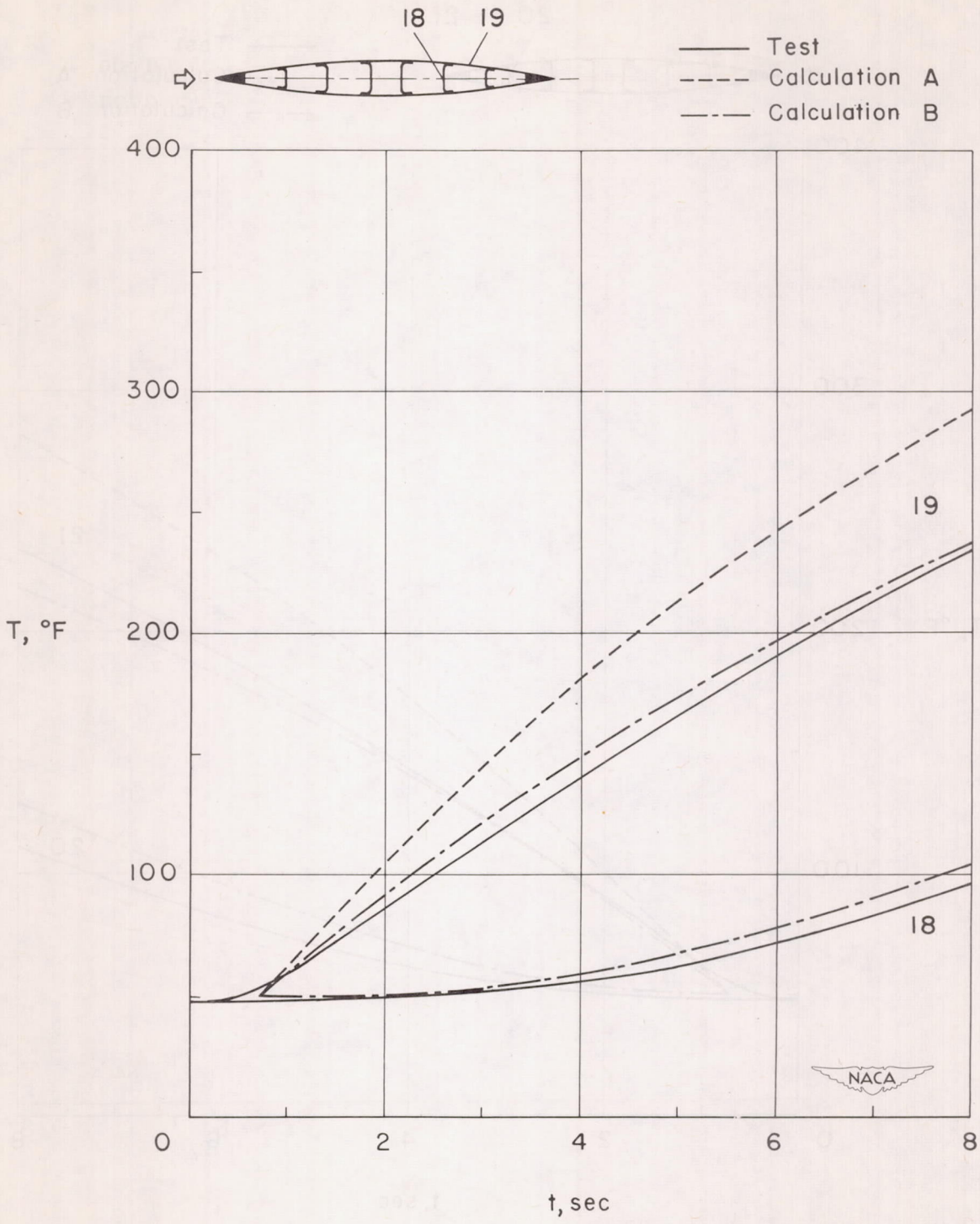

(g) Thermocouples 18 and 19.

Figure 8.- Continued.

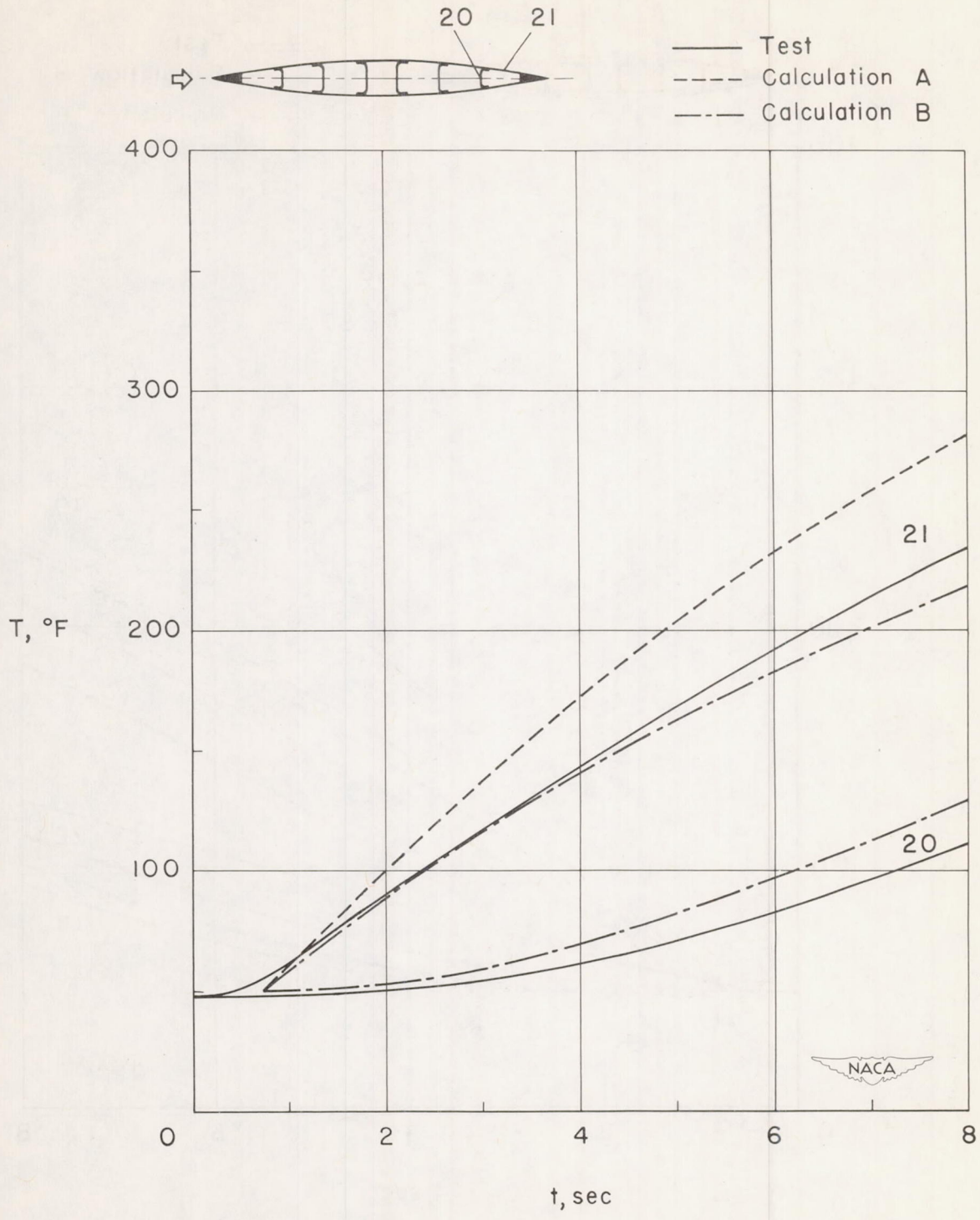

(h) Thermocouples 20 and 21.

Figure 8.- Continued.

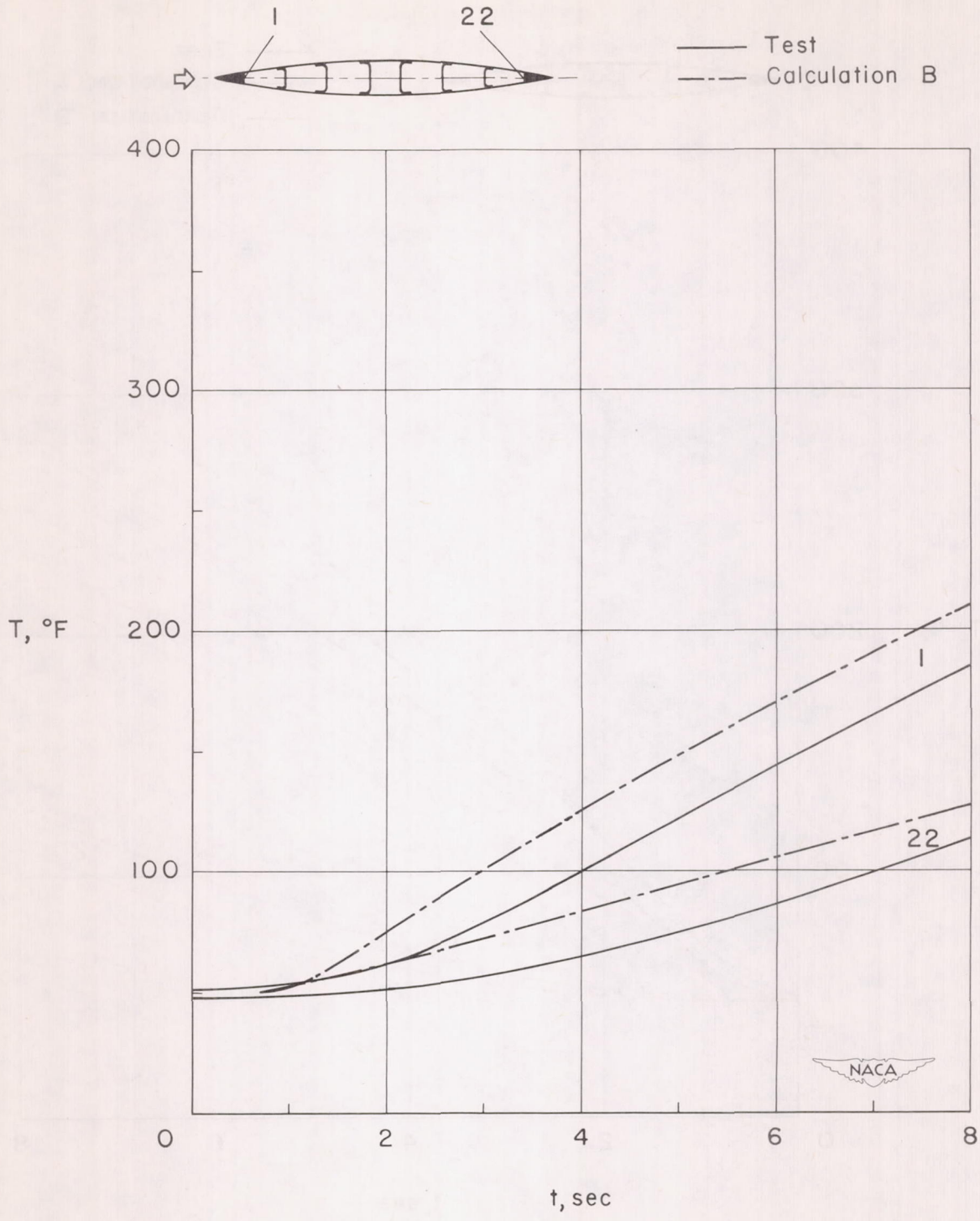

(i) Thermocouples 1 and 22.

Figure 8.- Continued.

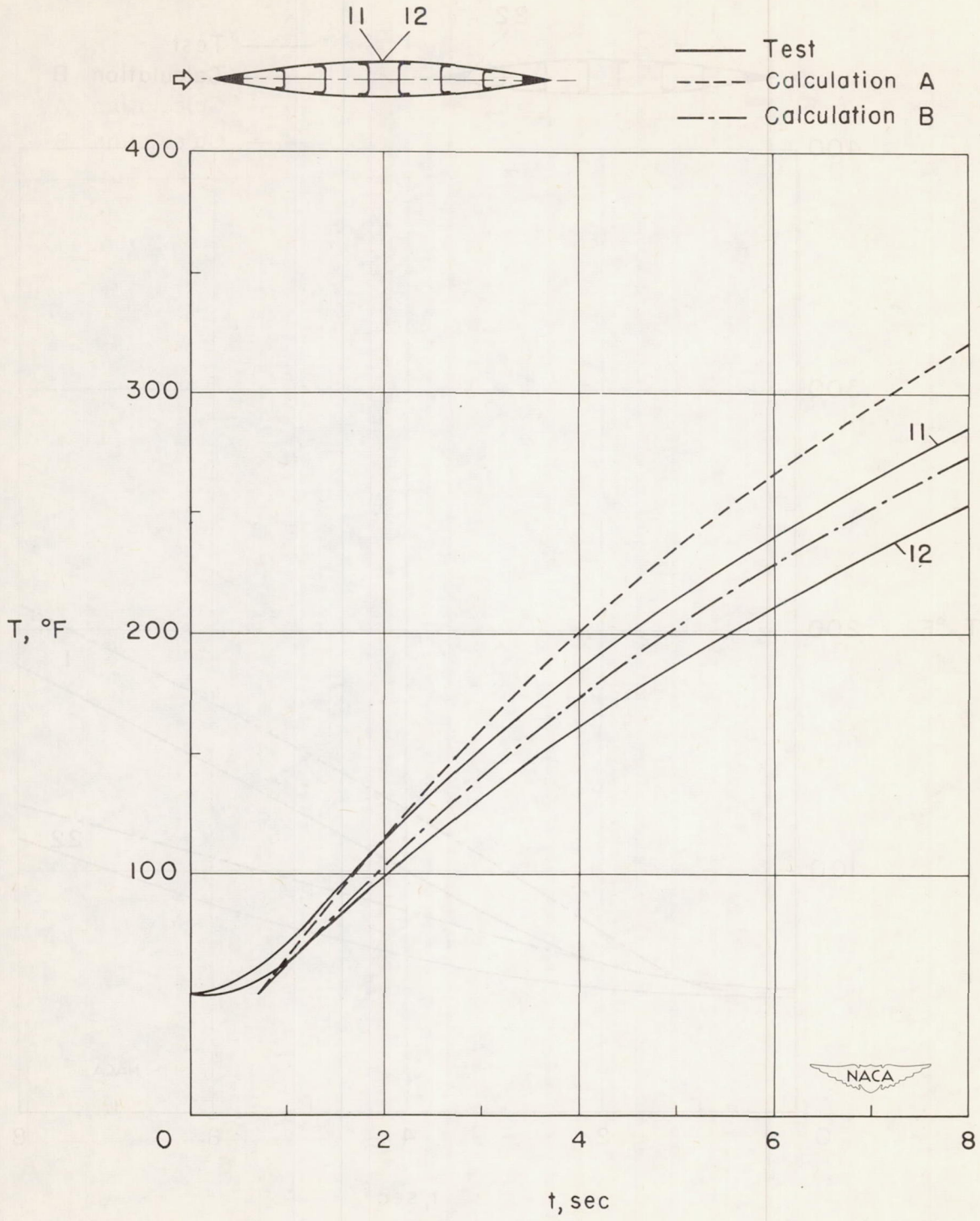

(j) Thermocouples 11 and 12.

Figure 8.- Continued.

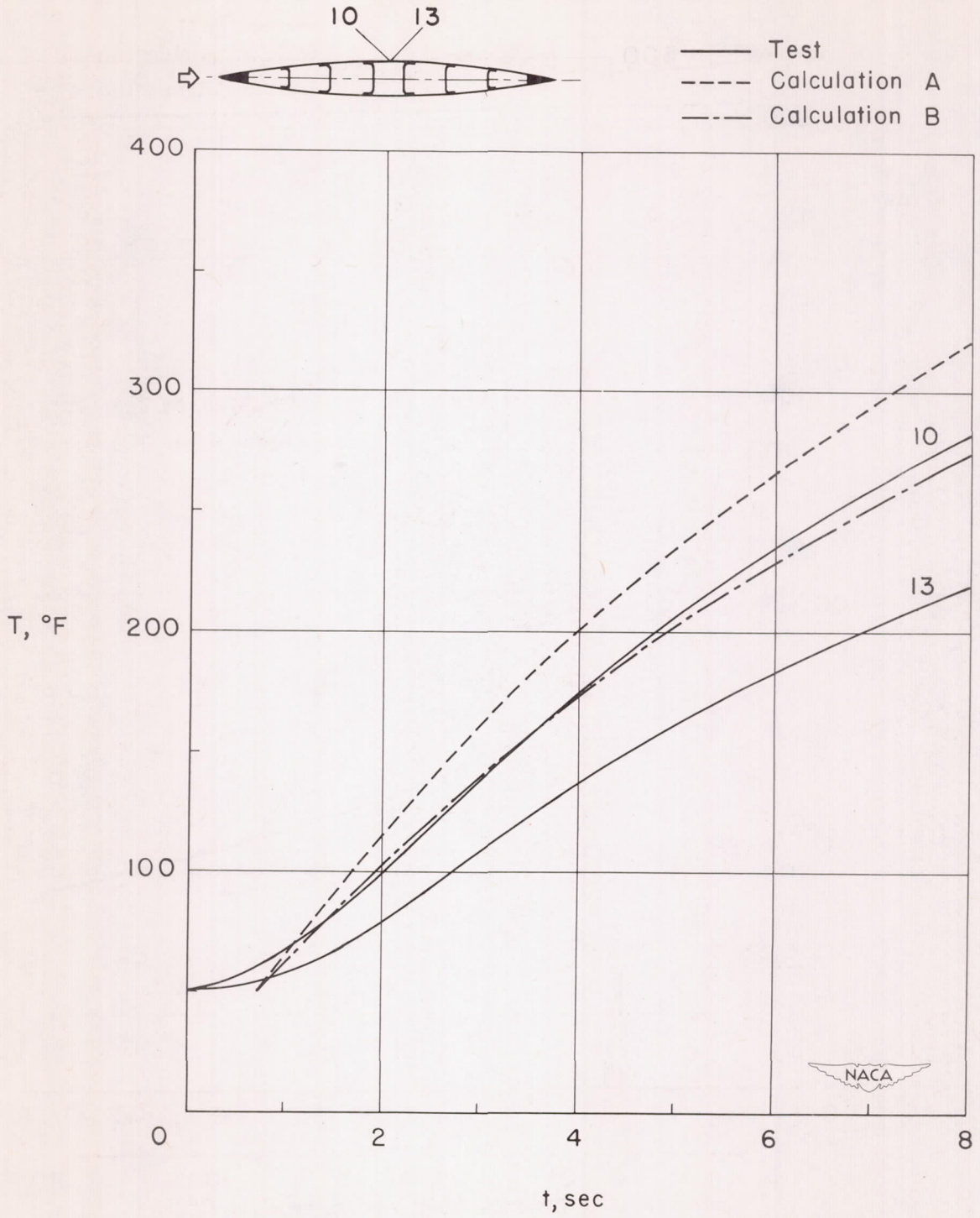

(k) Thermocouples 10 and 13.

Figure 8.- Concluded.

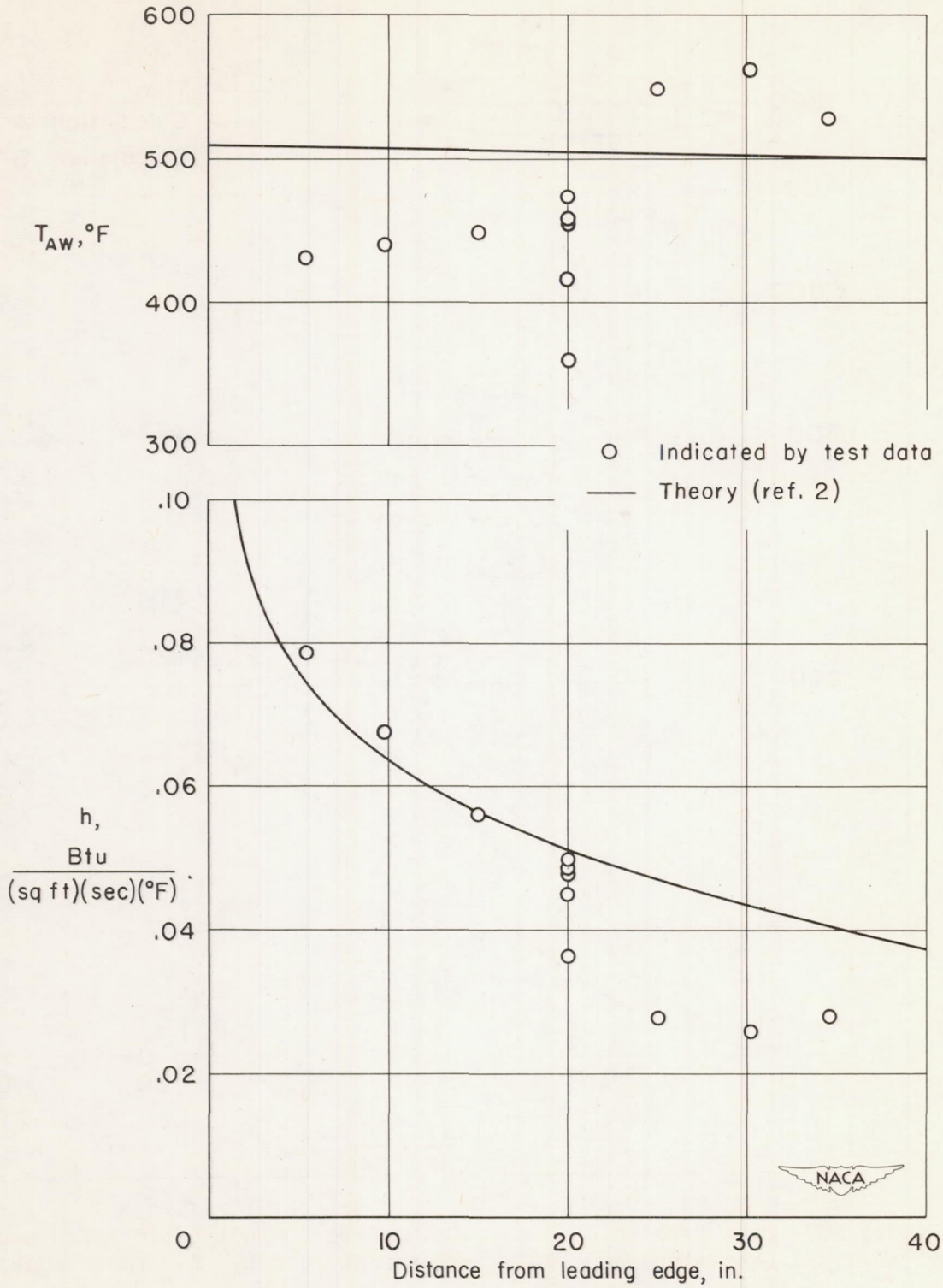

Figure 9.- Chordwise variation of adiabatic wall temperature and heat-transfer coefficient.

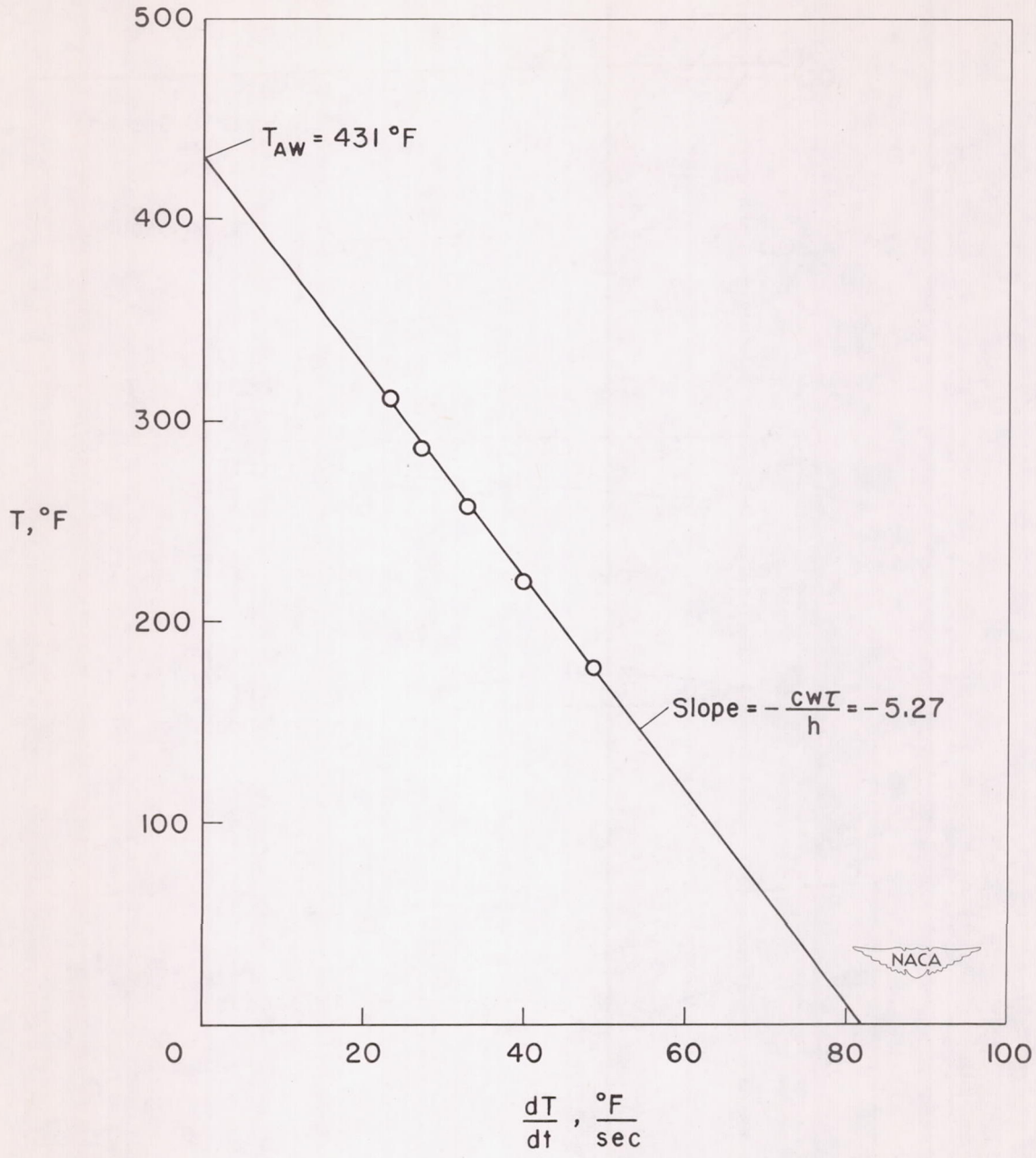

Figure 10.- Plot from which "indicated" values of adiabatic wall temperature and heat-transfer coefficient can be obtained for thermocouple 2.

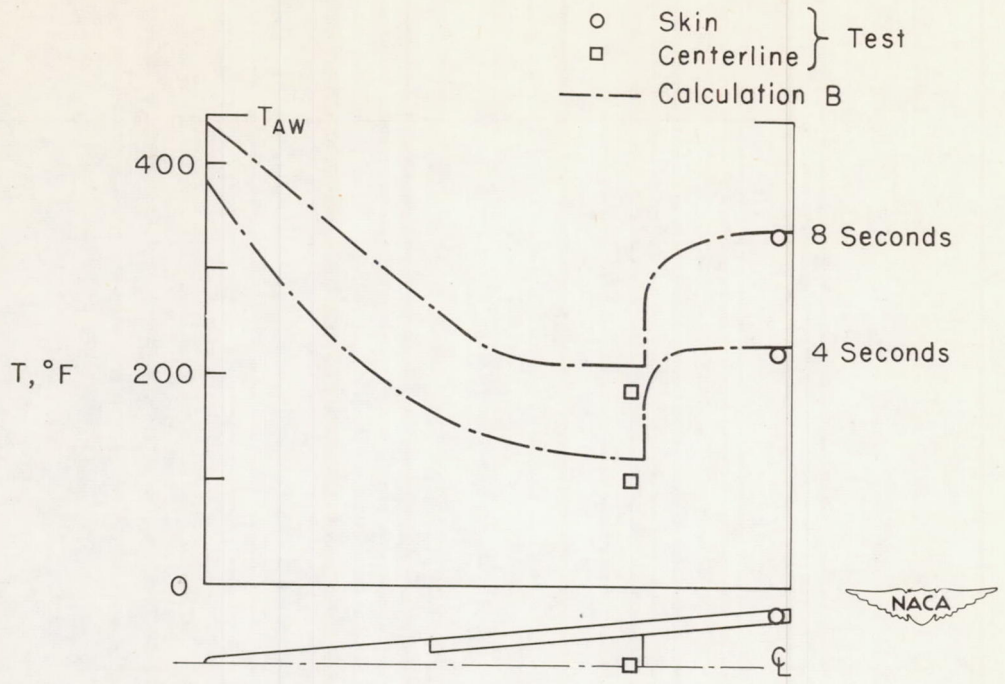

Figure 11.- Temperature distributions in leading-edge section.

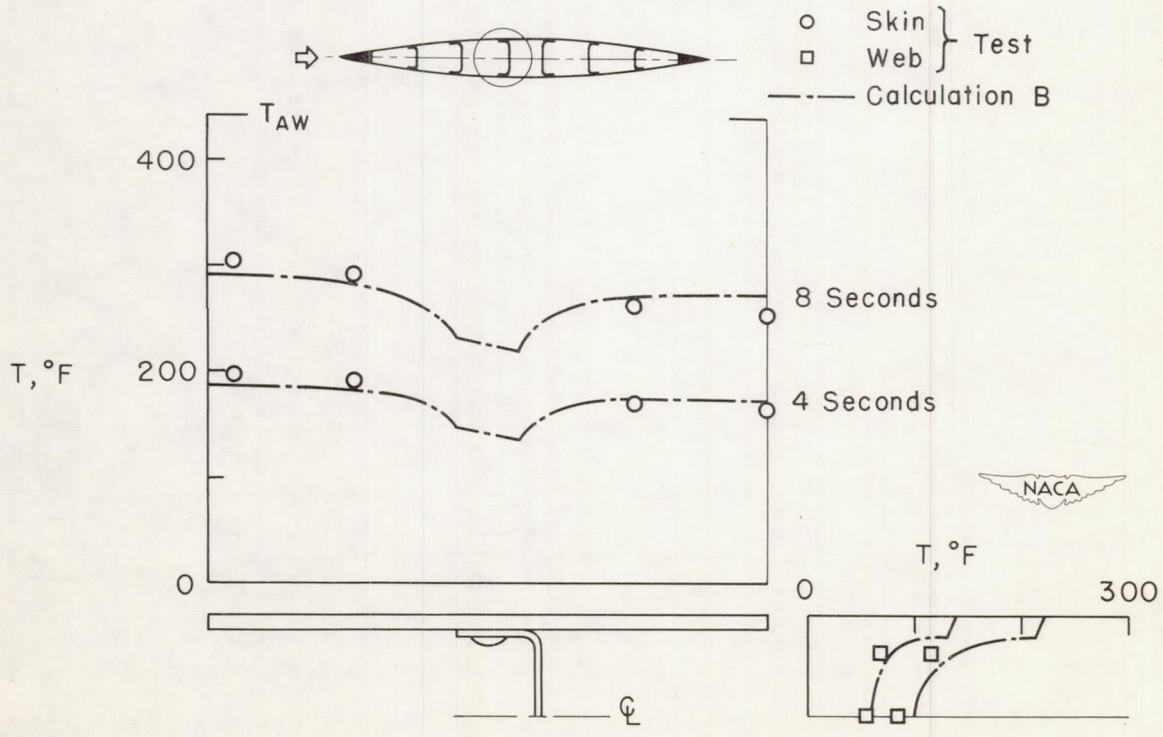

Figure 12.- Skin and web temperature distributions.

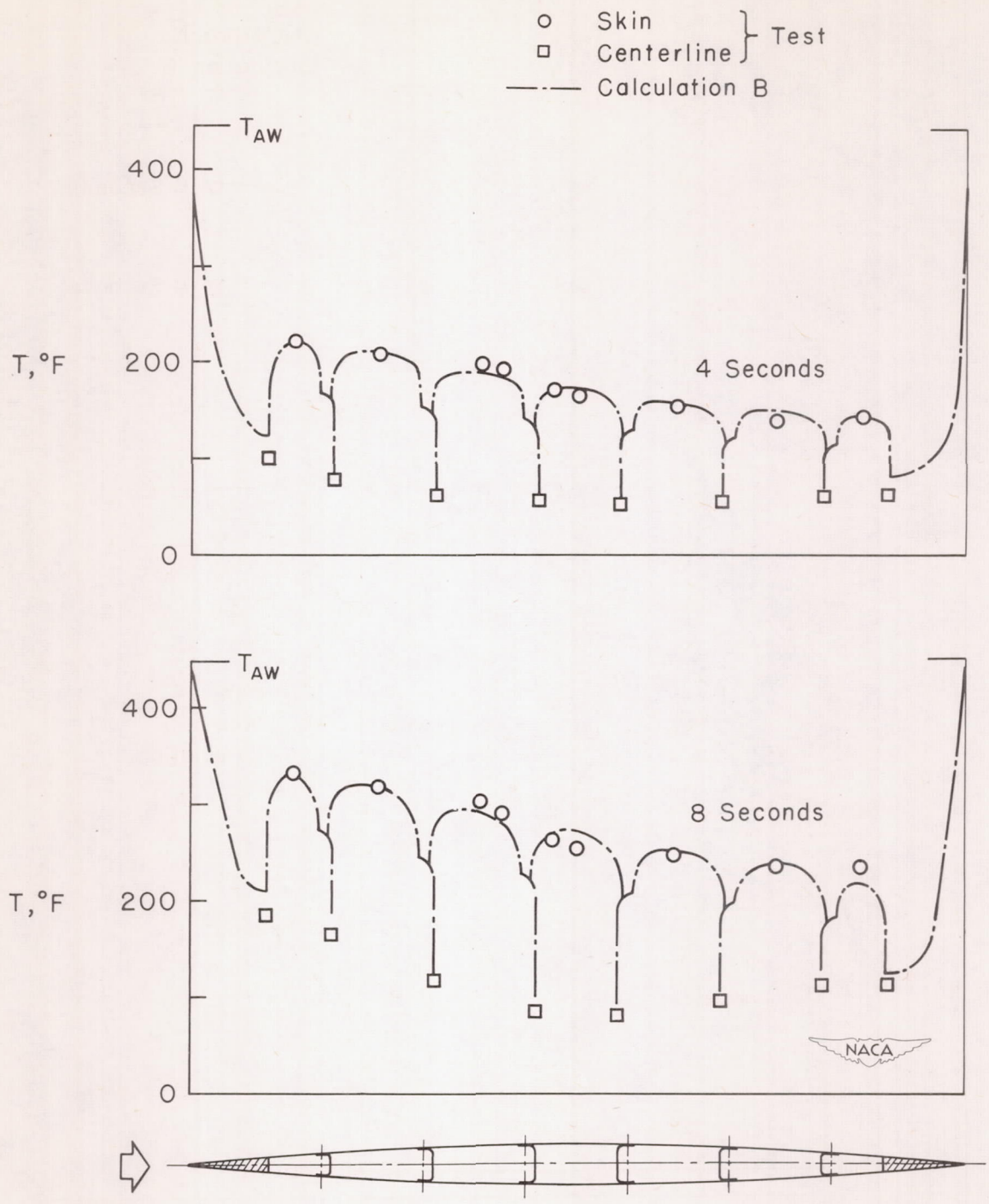

Figure 13.- Temperature distribution of entire cross section.